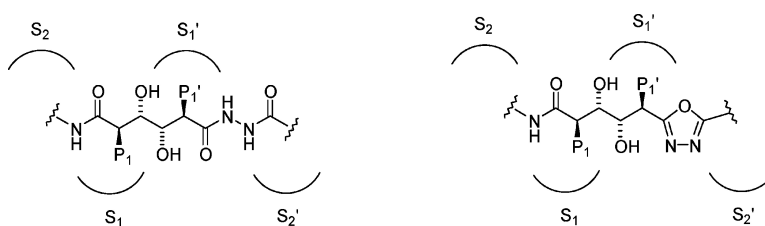


Synthesis of Malarial Plasmeepsin Inhibitors and Prediction of Binding Modes by Molecular Dynamics Simulations

Karolina Ersmark, Martin Nervall, Elizabeth Hamelink, Linda K. Janka, Jose C. Clemente, Ben M. Dunn, Michael J. Blackman, Bertil Samuelsson, Johan qvist, and Anders Hallberg

J. Med. Chem., **2005**, 48 (19), 6090-6106 • DOI: 10.1021/jm050463I • Publication Date (Web): 23 August 2005

Downloaded from <http://pubs.acs.org> on March 28, 2009



More About This Article

Additional resources and features associated with this article are available within the HTML version:

- Supporting Information
- Links to the 5 articles that cite this article, as of the time of this article download
- Access to high resolution figures
- Links to articles and content related to this article
- Copyright permission to reproduce figures and/or text from this article

[View the Full Text HTML](#)

Synthesis of Malarial Plasmepsin Inhibitors and Prediction of Binding Modes by Molecular Dynamics Simulations

Karolina Ersmark,[†] Martin Nervall,[‡] Elizabeth Hamelink,[§] Linda K. Janka,[#] Jose C. Clemente,[#] Ben M. Dunn,[#] Michael J. Blackman,[⊥] Bertil Samuelsson,[§] Johan Åqvist,[‡] and Anders Hallberg^{*,†}

Department of Medicinal Chemistry, Uppsala University, BMC, Box 574, 751 23 Uppsala, Sweden, Department of Cell and Molecular Biology, Uppsala University, BMC, Box 596, 751 24 Uppsala, Sweden, Division of Parasitology, National Institute for Medical Research, The Ridgeway, Mill Hill, London NW1 1AA, UK, Medivir AB, Lunastigen 7, 141 44 Huddinge, Sweden, and Department of Biochemistry and Molecular Biology, University of Florida College of Medicine, P.O. Box 100245 Gainesville, Florida 32610-0245

Received May 17, 2005

A series of inhibitors of the malarial aspartic proteases Plm I and II have been synthesized with L-mannitol as precursor. These inhibitors are characterized by either a diacylhydrazine or a five-membered oxadiazole ring replacing backbone amide functionalities. Molecular dynamics simulations were applied in the design process. The computationally predicted Plm II K_i values were generally in excellent agreement with the biological results. The diacylhydrazine was found to be superior over the oxadiazole as an amide bond replacement in the Plm I and II inhibitors studied. An extensive flexibility of the S2' pocket was captured by the simulations predicting the binding mode of the unsymmetrical inhibitors. Plm I and II inhibitors with single digit nanomolar K_i values devoid of inhibitory activity toward human Cat D were identified. One compound, lacking amide bonds, was found to be Plm IV selective and very potent, with a K_i value of 35 nM.

Introduction

Malaria, one of the most serious infectious diseases in the world, is caused by protozoan parasites of the genus *Plasmodium*. Of the four human species, *Plasmodium falciparum* is by far the most lethal and is responsible for the majority of the estimated 0.7–2.7 million malaria related deaths occurring annually.¹ Currently, there is a rapid spread of parasite drug resistance, mainly among the *P. falciparum* strains, resulting in an urgent need for new effective drugs with new mechanisms of action.² The publication of the *P. falciparum* genome has revealed a number of new targets for drug development.³ Among these are the hemoglobin degrading aspartic proteases plasmepsin I, II and IV (Plm I, II and IV) and the closely related histoaspartic protease (HAP).⁴ It has been shown that hemoglobin catabolism, which takes place in an acidic food vacuole, is essential for parasite survival both in culture and in animal models.^{5–7} Besides aspartic proteases three cysteine proteases (falcipain-1, -2, and -3) and one metallo protease (falcilysin) have also been identified to digest hemoglobin in the food vacuole.^{8–11} Until now Plm I and II have been most extensively studied of the four aspartic proteases, but there is a growing interest in the recently characterized Plm IV and HAP.^{12–15} Plm I and II demonstrate the highest sequence homology and are both involved in the initial cleavage of the native hemoglobin.^{16–18} Several potent

inhibitors of Plm I and II have been identified.^{7,12,19–34} However, achieving selectivity versus the highly homologous human aspartic protease cathepsin D (Cat D), and activity in parasite infected red blood cells have emerged as major challenges.^{7,35}

Directed by binding affinity calculations using the linear interaction energy (LIE) method, we previously reported the design of a series of C_2 -symmetric inhibitors with high affinities to both Plm I and II ($K_i = 0.5–37$ nM and 6–181 nM, respectively).²⁶ Notably, all of the inhibitors demonstrated a unique selectivity versus the human Cat D ($K_i > 2000$ nM).²⁶ The characteristic features of these inhibitors were (a) a 1,2-dihydroxyethylene unit mimicking the tetrahedral intermediate in the enzymatic cleavage and (b) two extended P1/P1' side chains designed to interact with the unobstructed S1–S3 cleft and the flexible S1' region. Despite high affinities in plasmepsin assays, the inhibitors exerted moderate inhibition of parasite growth in red blood cells.²⁶

Application of the concept of bioisosteric replacement is an established strategy to circumvent undesirable ADME profiles and has been extensively used as an approach to optimize lead compounds in drug discovery.^{36,37} In conversions of peptides to peptide mimetics the amide bonds are often replaced.^{36–38} The suitability of the replacing groups as bioisosteres depend on the role of the amide in the molecular recognition, i.e., if the amide group acts as a hydrogen bond donor and/or acceptor or if it solely acts as a spacer when the molecule interacts with its receptor.

Both experimental crystal structures^{21,33,39} and molecular dynamics (MD) simulations^{26,27} indicate that the Plm II binding cleft is quite flexible and can accommodate ligands with P1/P1' and P2/P2' substituents of

* To whom correspondence should be addressed. E-mail: Anders.Hallberg@orgfarm.uu.se. Phone: +46-18471 42 84, Fax: +46-18 471 44 74.

[†] Department of Medicinal Chemistry, Uppsala University.

[‡] Department of Cell and Molecular Biology, Uppsala University.

[⊥] National Institute for Medical Research.

[§] Medivir AB.

[#] University of Florida College of Medicine.

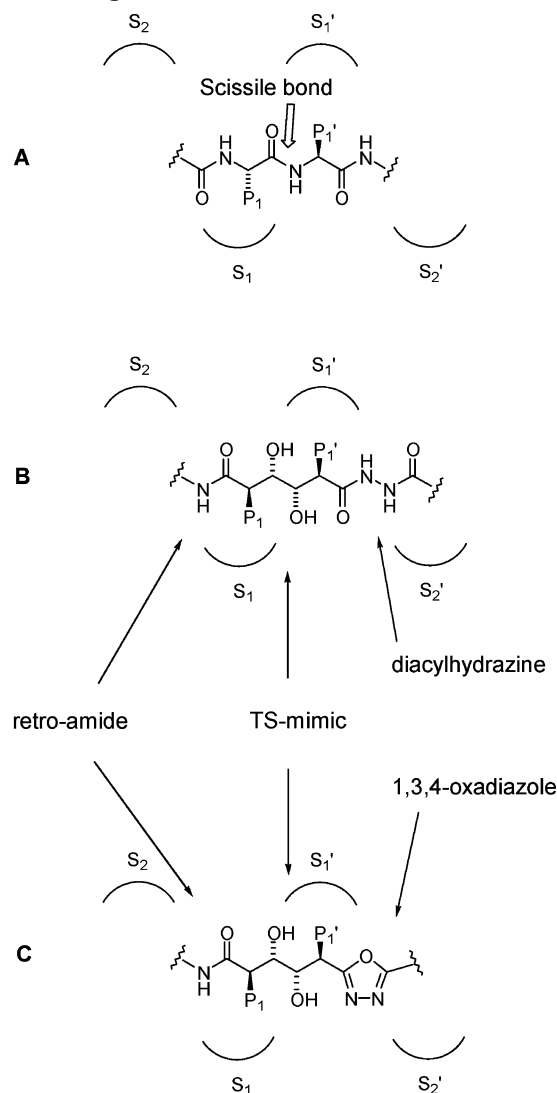
varying size. Such a situation generally makes automated docking procedures less reliable if the receptor protein is treated as rigid, which is often the case. Hence, automated docking of our earlier series of inhibitors using the X-ray structure of the Plm II-pepstatin complex was not successful. On the other hand, we found that superposition of the inhibitor scaffolds combined with subsequent relaxation by MD simulations produced reasonable structures as judged both by their energetics and by comparison to independent crystallographic results.²⁷ Thus, MD simulations in combination with the linear interaction energy (LIE) method resulted in theoretical binding affinities in excellent agreement with experimental measurements when the C_2 -symmetric inhibitors were investigated.^{26,27}

Herein, we report the impact of replacing one or both of the two amide bonds of the previously reported C_2 -symmetric inhibitors,²⁶ by either (a) a diacylhydrazine element with ability to participate in an extensive hydrogen bond network or (b) a compact 1,3,4-oxadiazole possessing only hydrogen bond accepting capacity. The characteristic features of the central core structure of the unsymmetrical inhibitors are illustrated in Chart 1. The design that delivered potent and selective Plm I/Plm II inhibitors with no inhibition of the human Cat D used a bisvinyl bromide as a starting structure and was partly guided by MD simulations with Plm II as target enzyme. Furthermore, we report computational predictions of the binding conformations for these unsymmetrical inhibitors.

Results

Chemistry. The synthetic routes to the symmetrical (**3** and **4**) and to the unsymmetrical (**5–13** and **16**) diacylhydrazine inhibitors as well as to the 1,3,4-oxadiazole inhibitors (symmetrical **17** and **18** and unsymmetrical **19–24**) are outlined in Scheme 1. The vinyl bromide fragments were intended to serve as suitable handles for further transformations. The precursor bislactones **26** and **27** were prepared as described previously.²⁶ To produce the symmetrical diacylhydrazines, **3** and **4**, an excess of hydrazide was used to open the bislactone rings of **27**. Subsequent dehydration of the corresponding diacylhydrazine using Burgess reagent⁴⁰ delivered the symmetrical 1,3,4-oxadiazoles **17** and **18**. To avoid reaction between Burgess reagent and the hydroxyl groups, protection with chlorotrimethylsilane was first performed and the cyclodehydration was thereafter accomplished with Burgess reagent. Deprotection using potassium fluoride gave the 1,3,4-oxadiazoles (**17** and **18**). The unsymmetrical compounds were easily available from the monolactone intermediates **28** and **29** (Scheme 1). Mono opening of the bislactones **26** or **27** with (1*S*,2*R*)-1-amino-2-indanol could be achieved essentially as previously reported for a benzyloxy analogue utilizing 2-hydroxypyridine as catalyst to deliver the monolactones **28** and **29**.⁴¹ Ring opening of the monolactone (**28** or **29**) using an excess of hydrazide gave the unsymmetrical diacylhydrazines **5–13** and **16**. The unsymmetrical 1,3,4-oxadiazoles **19–24** were then obtained by a similar procedure as used for the preparation of the symmetrical 1,3,4-oxadiazoles. Thus, the alcohols were first protected with chlorotrimethylsilane and subsequent cyclodehydration with Burgess reagent

Chart 1. Generic Structures of Plm II Substrate (A) and Two Inhibitors (B and C) Encompassing TS-Mimicking Scaffolds Derived from L-Mannitol

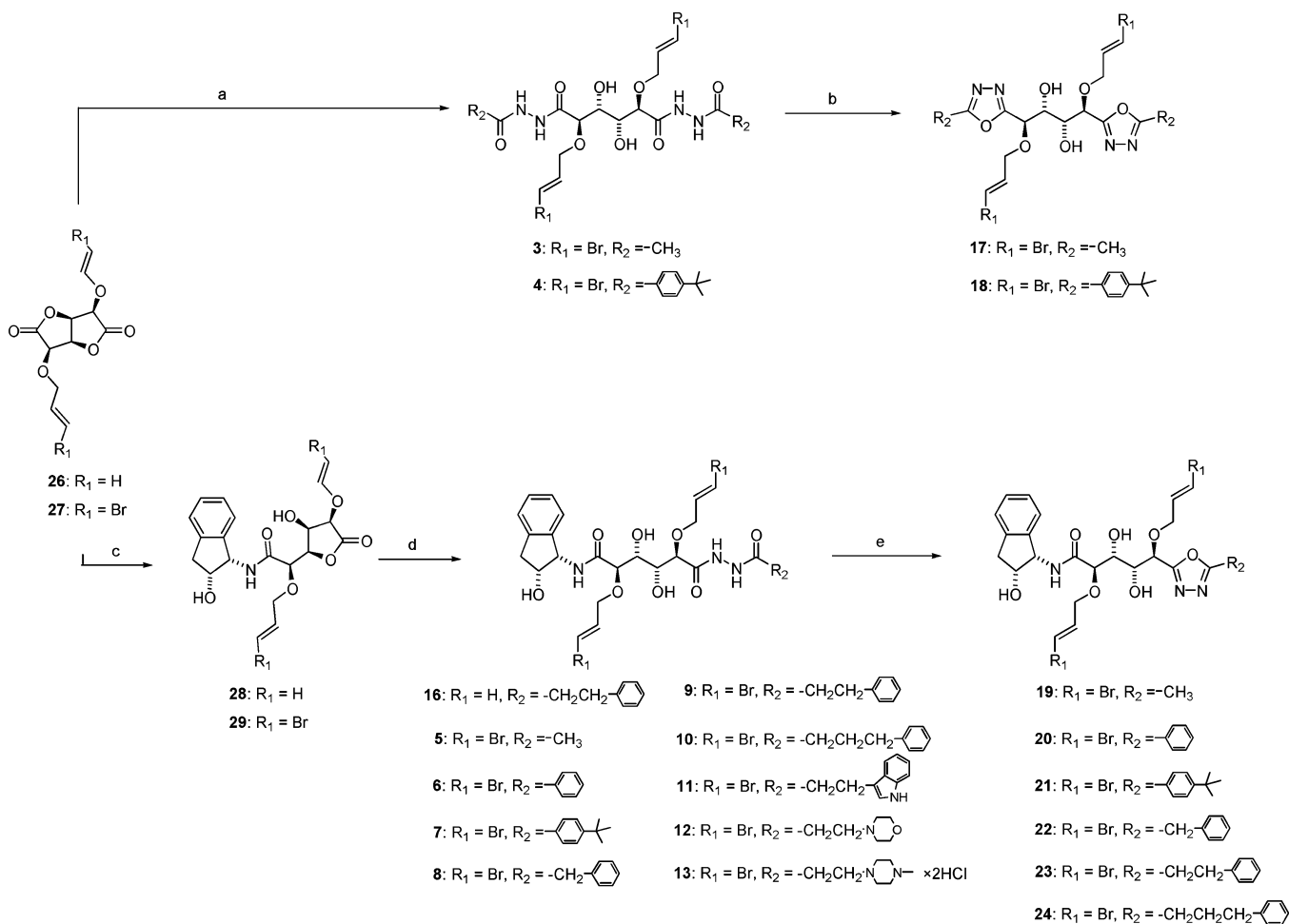


and deprotection delivered the unsymmetrical 1,3,4-oxadiazoles **19–24** in moderate to good yields over three steps (20–70%).

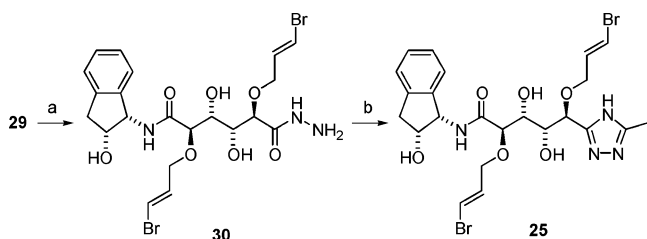
The 1,2,4-triazole **25** was generated in two steps from the monolactone intermediate **29** (Scheme 2). Nucleophilic ring opening of the monolactone with hydrazine hydrate furnished the corresponding hydrazide **30**. Condensation of the hydrazide **30** with acetamidine, to the amidrazone (not isolated), followed by thermal cyclization provided eventually the 1,2,4-triazole **25**.

For the preparation of the unsymmetrical diacylhydrazine analogues **14** and **15** with extended P₁/P_{1'} arms, microwave-assisted Suzuki couplings were conducted (Scheme 3).^{42,43} The (*E*)-bromo diacylhydrazine precursor **9** was reacted with an excess of the appropriate organoboronic acid, a catalytic amount of Pd₂(dba)₃/[(*t*-Bu)₃PH]BF₄,⁴⁴ and Ba(OH)₂ as a base. Microwave irradiation at 110 °C for 15 min furnished the (*E*)-methylenedioxyphenyl compound **14**. With the less reactive electron-poor acetylphenylboronic acid as reactant the reaction time had to be prolonged to 40 min to obtain the (*E*)-acetylphenyl compound **15**.

Although a small optimization of the reaction protocol was made, **14** and **15** were both isolated in low yields

Scheme 1^a

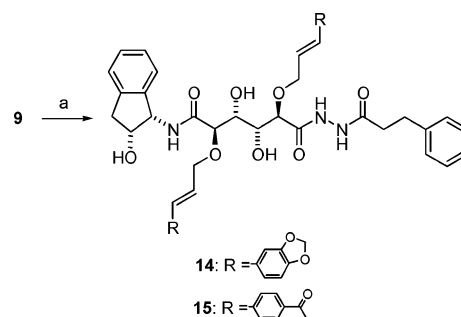
^a (a) R₂CONHNH₂, CH₂Cl₂, reflux; (b) i. TMSCl, NEt₃, CH₂Cl₂ ii. Burgess reagent, THF, reflux iii. KF·2H₂O; (c) (1*S*,2*R*)-1-amino-2-indanol, 2-hydroxypyridine, CH₂Cl₂ (d) R₂CONHNH₂, CH₂Cl₂, reflux; (e) i. TMSCl, NEt₃, CH₂Cl₂ ii. Burgess reagent, THF, reflux iii. KF·2H₂O.

Scheme 2^a

^a (a) NH₂NH₂·H₂O, EtOH (b) CH₃CNHNH₂, EtOH, reflux.

(23% and 22%, respectively). Initial attempts with Pd(PPh₃)₄ as catalyst and Na₂CO₃ as a base were unsuccessful in producing full consumption of the starting material and significant mono- and di-dehalogenation occurred as deduced from analytical RP-LC-MS. The change of base to Ba(OH)₂ × 8H₂O increased the reaction rate and produced less dehalogenation. However, the chromatographic purification was found very difficult, partly due to triphenylphosphine oxide contaminations. This problem was circumvented by the use of a different catalyst system, (Pd₂(dba)₃/[(*t*-Bu)₃PH]BF₄), exhibiting a comparable catalytic activity.

Enzyme Inhibition. The inhibitory activities and the selectivity of the compounds **3–25** were determined in Plm I, Plm II, and Cat D enzyme assays, and the results are summarized as *K*_i values in Table 1. The two

Scheme 3^a

^a (a) RB(OH)₂, Pd₂(dba)₃/[(*t*-Bu)₃PH]BF₄, Ba(OH)₂·8H₂O, DME, H₂O, EtOH, microwave irradiation.

symmetrical diamides **1** and **2**, both previously prepared,²⁶ were included as reference compounds. Overall, the symmetrical inhibitors (**3** and **4** and **17** and **18**) were less potent than the unsymmetrical (**5–16** and **19–25**). Among the symmetrical compounds only the diacylhydrazine with a 4-*tert*-butylphenyl **4** demonstrated any affinity in the Plm I and II assays. A comparison between the two amide bond replacing groups, the extended diacylhydrazine and the compact 1,3,4-oxadiazole, revealed that the diacylhydrazine is far superior over the oxadiazole. The 1,3,4-oxadiazoles exhibited *K*_i values, at the best in the micromolar range, and only one of these compounds, **24**, was active in the Plm I

Table 1. Plasmeprin Inhibitory Activity of the Prepared Compounds Encompassing Amide Bond Replacements

Compound	Structure	Enzyme K_i (nM)			Cat D
		Plm I	Plm II		
			expt	calc ^a	
1 ^b		163 ^c	96 ^d	240 ^d	>2000 ^e
2		27 ^c	47 ^c	150	>2000 ^e
3		>3000	>5000	nd	>6000
4 ^e		1837	1500	nd	3000
5		698	359	737	>6000
6		261	168	nd	>6000
7		198	142	nd	>6000
8		31	14	nd	>6000

Table 1 (Continued)

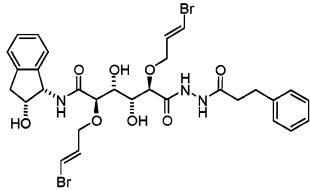
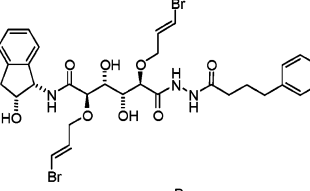
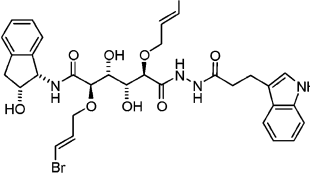
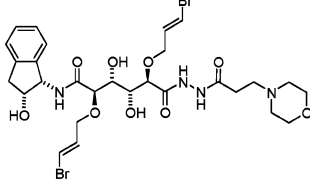
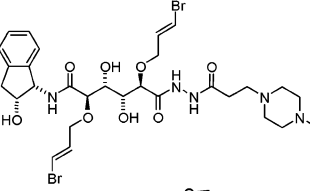
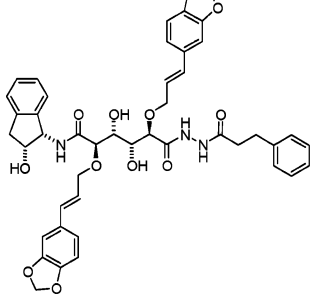
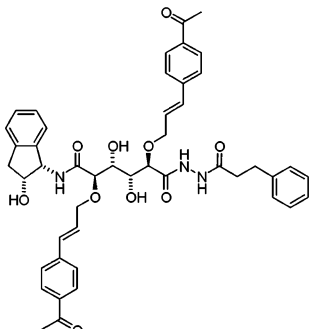
Compound	Structure	Enzyme K_i (nM)			Cat D
		Plm I	Plm II		
			expt	calc ^a	
9		9	7	36	>6000
10		11	10	nd	>6000
11		19	6	nd	>6000
12		2000	1300	nd	>6000
13		1090	586	nd	>6000
14		6	11	20	800
15		38	145	12	1200

Table 1 (Continued)

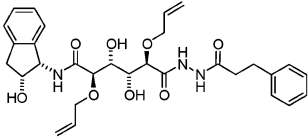
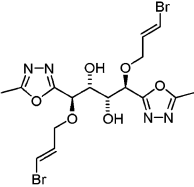
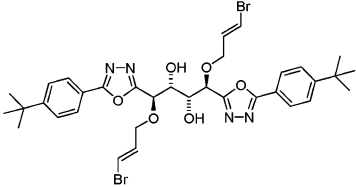
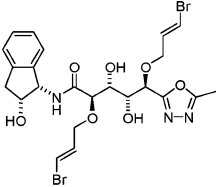
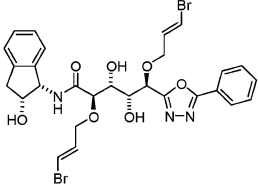
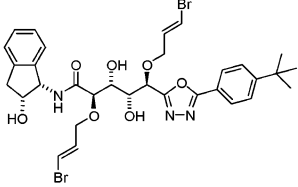
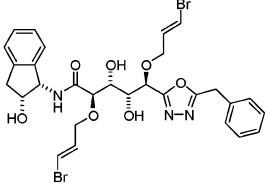
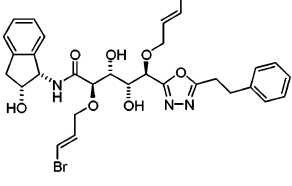
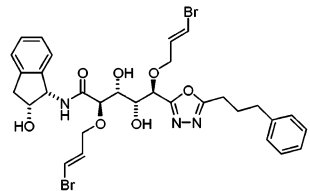
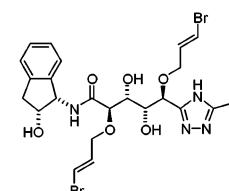
Compound	Structure	Enzyme K_i (nM)			
		Plm I	Plm II		Cat D
			expt	calc ^a	
16		124	161	91	>6000
17		>3000	>5000	nd	>6000
18 ^f		>3000	>5000	nd	>6000
19		>3000	>5000	10000	>6000
20		>3000	3400	nd	>6000
21		>3000	>5000	nd	>6000
22		>3000	2100	nd	>6000
23		>3000	2900	728	>6000

Table 1 (Continued)

Compound	Structure	Enzyme K_i (nM)			
		Plm I	Plm II		Cat D
			expt	calc ^a	
24		1600	2300	nd	>6000
25		>3000	>5000	nd	>6000

^a nd, not determined. ^b K_i Plm IV, >5000 nM. ^c Data from ref 26. ^d Data from ref 27. ^e K_i Plm IV, 478 nM. ^f K_i Plm IV, 35 nM. Inhibition on *P. falciparum* infected red blood cells; 25% inhibition at 4 μ M.

assay, while several of the diacylhydrazines demonstrated K_i values in the low nanomolar range in both Plm I and II assays. The 1,2,4-triazole compound **25** was employed as a reference compound encompassing in contrast to **19**, a five-membered heterocycle with a hydrogen bond donating NH. However, incorporation of this heterocycle rendered a compound inactive in all enzyme assays assessed, as was the case with **19**.

The importance of the size of the P2' side chain is demonstrated in Table 1. Thus, replacing a methyl (**5**) by a phenyl (**6**) and a 4-*tert*-butylphenyl group (**7**) generated consistently more potent unsymmetrical diacylhydrazine Plm I and II inhibitors. Among the unsymmetrical oxadiazoles with these three P2' side chains, only the phenyl derivative **20** exhibited any inhibitory activity for Plm II (cf. **19**, **20**, and **21**). Introducing an extended spacer arm and flexibility (**8–10** and **22–24**) further improved the inhibitory potency. The effect was most pronounced with the diacylhydrazines (**8–10**), but the inhibitors with a 1,3,4-oxadiazole were still weak (**22–24**). A two-carbon extension (**9**) between the diacylhydrazine and a phenyl seemed optimal and gave rise to potencies three times higher in the Plm I assay and almost seven times higher in the Plm II assay ($K_i = 9$ nM and 7 nM, respectively), compared to the parent compound **2** ($K_i = 27$ nM and 47 nM, respectively). Saturated basic nitrogen ring systems at the same distance to the diacylhydrazine (the morpholine **12** and the piperazine **13**) resulted in a substantial loss in affinity.

Surprisingly, an elongation of the P1/P1' side chains did not render the same positive impact as previously observed in a series of related C_2 -symmetric inhibitors (cf. **9** with **14–15**).²⁶ Hence, the extended methylenedioxyphenyl **14** demonstrated almost the same potency as the corresponding bis(vinyl bromide) **9**, and the acetylphenyl extension in **15** gave a significantly lower activity. A shorter P1 and P1' side chain, as in the allyloxy derivative **16**, provided a less potent inhibitor. All P1/P1' bis(vinyl bromide)-containing compounds,

except the oxadiazole **24**, were more active in the Plm II than in the Plm I assay.

Three of the compounds (**1**, **4**, and **18**) were examined in a Plm IV assay, and the K_i values are reported as footnotes to Table 1. The allyloxy inhibitor **1** was found inactive, but the diacylhydrazine **4** and the 1,3,4-oxadiazole **18** exhibited a much higher potency in the Plm IV assay than what was observed in the Plm I and II assays (Plm IV $K_i = 478$ nM and 35 nM, respectively). Notably, the Plm IV selective symmetrical nonpeptidic inhibitor **18** demonstrated a 25% inhibition of parasite growth in infected erythrocytes at 4 μ M.

In general, the inhibitors did not exhibit Cat D binding, although the symmetrical diacylhydrazine **4** and the two phenethyl diacylhydrazine inhibitors, **14** and **15**, demonstrated a weak binding to the mammalian enzyme ($K_i = 3000$ nM, 800 nM, and 1200 nM, respectively).

Molecular Dynamics Simulations and Free Energy Calculations. The binding of seven of the synthesized compounds and the previously prepared diamide **2** were analyzed by computer simulation methods. Binding free energies of **2**, **5**, **9**, **14–16**, **19** and **23** to Plm II were estimated with the linear interaction energy (LIE) method⁴⁵ and complementary docking studies were carried out with Autodock.⁴⁶

As previously reported with similar compounds,²⁷ rigid receptor automated docking with Autodock is problematic due to the flexible nature of the Plm II binding site. To solve the problem of getting reasonable starting structures for molecular dynamics (MD) simulations, the ligands were superimposed onto the scaffold of compound **1** as modeled in an earlier study.²⁷ The template **1** is C_2 -symmetric whereas ligands **5**, **9**, **14–16**, **19** and **23** are only equivalent with regard to the P1/P1' positions. Two LIE calculations for each ligand were thus required to determine the favored binding mode, one with the diacylhydrazine or oxadiazole moiety on the prime side and one with these linkers on the nonprime side. A summary of the calculated data is

Table 2. Experimental and Calculated Energetics of Inhibition of Plm II

compound ^a	$\Delta G_{\text{bind, exp}}$ (kcal/mol) ^b	$\Delta G_{\text{bind, calc}}$ (kcal/mol)	ligand-surrounding interactions (kcal/mol) ^c			
			$\langle V_{\text{l-s}}^{\text{ndw}} \rangle_{\text{p}}$	$\langle V_{\text{l-s}}^{\text{el}} \rangle_{\text{p}}$	$\langle V_{\text{l-s}}^{\text{ndw}} \rangle_{\text{w}}$	$\langle V_{\text{l-s}}^{\text{el}} \rangle_{\text{w}}$
1 ^d	-9.6	-9.1 ± 0.4	-85.9 ± 0.1	-67.2 ± 0.1	-40.6 ± 0.1	-64.5 ± 0.9
2	-10.1	-9.4 ± 1.0	-102.6 ± 2.6	-74.0 ± 0.4	-49.6 ± 0.9	-74.7 ± 0.7
5 _{conf.1}	-8.9	-7.7 ± 0.7	-90.6 ± 1.3	-72.0 ± 0.2	-46.4 ± 0.2	-72.9 ± 1.0
5 _{conf.2}	-8.9	-8.4 ± 0.8	-90.4 ± 0.6	-74.2 ± 1.1	-46.4 ± 0.2	-72.9 ± 1.0
9 _{conf.1}	-11.2	-8.2 ± 0.9	-105.0 ± 2.0	-68.8 ± 0.3	-56.9 ± 0.7	-70.5 ± 0.9
9 _{conf.2}	-11.2	-10.2 ± 1.1	-108.2 ± 0.7	-73.3 ± 1.9	-56.9 ± 0.7	-70.5 ± 0.9
14 _{conf.1}	-10.9	-9.0 ± 1.0	-128.6 ± 0.7	-70.9 ± 0.7	-71.1 ± 0.5	-75.1 ± 1.8
14 _{conf.2}	-10.9	-10.6 ± 1.3	-128.5 ± 1.1	-75.7 ± 1.2	-71.1 ± 0.5	-75.1 ± 1.8
15 _{conf.1}	-9.4	-10.1 ± 0.8	-123.3 ± 0.6	-83.2 ± 0.5	-66.4 ± 1.6	-84.0 ± 0.9
15 _{conf.2}	-9.4	-10.9 ± 1.0	-127.5 ± 0.5	-83.4 ± 0.9	-66.4 ± 1.6	-84.0 ± 0.9
16 _{conf.1}	-9.3	-8.6 ± 0.4	-91.8 ± 0.1	-70.6 ± 0.4	-47.1 ± 0.1	-69.2 ± 0.9
16 _{conf.2}	-9.3	-9.7 ± 0.7	-94.8 ± 0.7	-72.3 ± 0.8	-47.1 ± 0.1	-69.2 ± 0.9
19 _{conf.1}	-7.3	-4.8 ± 0.6	-85.9 ± 1.4	-67.2 ± 0.6	-47.6 ± 0.4	-73.8 ± 0.2
19 _{conf.2}	-7.3	-6.9 ± 0.5	-87.4 ± 0.0	-72.7 ± 1.1	-47.6 ± 0.4	-73.8 ± 0.2
23 _{conf.1}	-7.6	-7.2 ± 0.5	-101.3 ± 0.5	-70.7 ± 1.0	-55.7 ± 0.3	-74.0 ± 0.1
23 _{conf.2}	-7.6	-8.4 ± 0.2	-103.3 ± 0.1	-73.4 ± 0.3	-55.7 ± 0.3	-74.0 ± 0.1

^a **conf.1** and **conf.2** indicate the different orientations of the inhibitor in the active site. In conformation **1** the diacylhydrazine or oxadiazole linker is on the nonprime side while in conformation **2** the diacylhydrazine or oxadiazole linker is on the prime side. ^b The experimental binding free energy calculated from experimentally determined K_{is} using $\Delta G_{\text{bind, exp}}^0 = RT \ln K_{\text{i}}$. ^c The calculated average electrostatic (V_{el}) and nonpolar (V_{ndw}) energies for ligand-surrounding (l-s) interactions. The subscripts p and w denote simulations of the ligand in complex with the protein and free in water, respectively. ^d Data from ref 27.

shown together with experimental data in Tables 1 and 2. It can be seen that both the absolute and relative binding free energies are rather well predicted by the simulations, and, in particular, one finds that the ranking with respect to the (minimal) P2' motif is correct, by comparing **2**, **5** and **19**. Furthermore, the favorable effect of the bromine substituent at the P1/P1' position (**2** vs **1** and **9** vs **16**) is also reproduced by the calculations.

Examination of how the electrostatic and hydrophobic contributions to the absolute binding affinity vary among the ligands reveals that the nonpolar (hydrophobic) term makes the dominating contribution for all the analyzed ligands. Furthermore, when comparing the two different binding directions we find that the most favored one, for all studied ligands, is with the diacylhydrazine/oxadiazole oriented to the prime side. The data in Table 2 also reveal that in all cases, except for **15**, the polar contribution is the main determinant of the favored binding direction. This is in accordance with the general notion that while hydrophobic binding provides most of the overall affinity, the polar interactions such as H-bonds confer specificity in enzyme-inhibitor complexes.^{27,47,48}

In the MD simulations of the ligand complexes the central scaffold (i.e. the six central atoms originating from mannitol) of the ligands adopts the same conformation as observed earlier.²⁶ Hence, the hydroxyl group adjacent to P1' makes the crucial transition state mimic interaction with the two active aspartic acids Asp34 and Asp214. The second central hydroxyl makes a very strong anionic H-bond interaction with Asp214 and also interacts with an active site water as found earlier.²⁶ The P1 group of the simulated ligands resides in the S1 pocket of Plm II. The larger P1 substituents in **14** and **15** stretch according to the simulation through the entire S1-S3 site, exposing the outermost part of the P1 group to the solvent. The P1' substituent reaches into the S1' site of the protein and causes a slight expansion of S1' by movements of the Phe294 side chain.

During simulation of **14** with the diacylhydrazine linker on the prime side we observed an expansion of

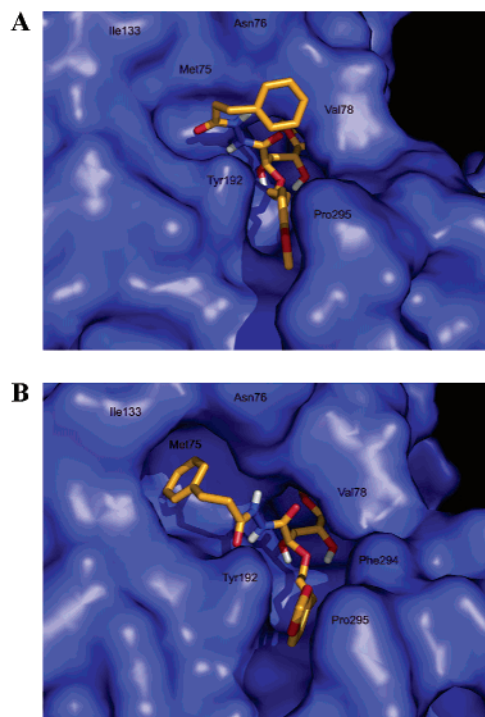


Figure 1. Surface representation of PlmII in complex with **14**: (A) Snapshot from MD simulations with the S2' subsite closed as in the starting structure and (B) after the S2' cavity has opened. The snug fit of the P2' phenyl group in the pocket can be seen, as well as the accompanying conformational change of the diacylhydrazine fragment that is necessary for the stable H-bond network seen in Figure 2.

the S2' pocket to fully accommodate the bulky phenyl moiety (Figure 1). The phenyl ring of **14** enters the expanded pocket after a few hundred picoseconds and stays there for the rest of the simulation (>2 ns). The observed flexibility in S2' is found to originate from movements of Met75. The backbone of the protein is not displaced significantly but the methionine side chain is rotated toward the interior of the enzyme, thereby opening S2' enough for the phenyl group to enter. It is notable that the conformational change of Met75 seen in the MD simulations is supported by experimental

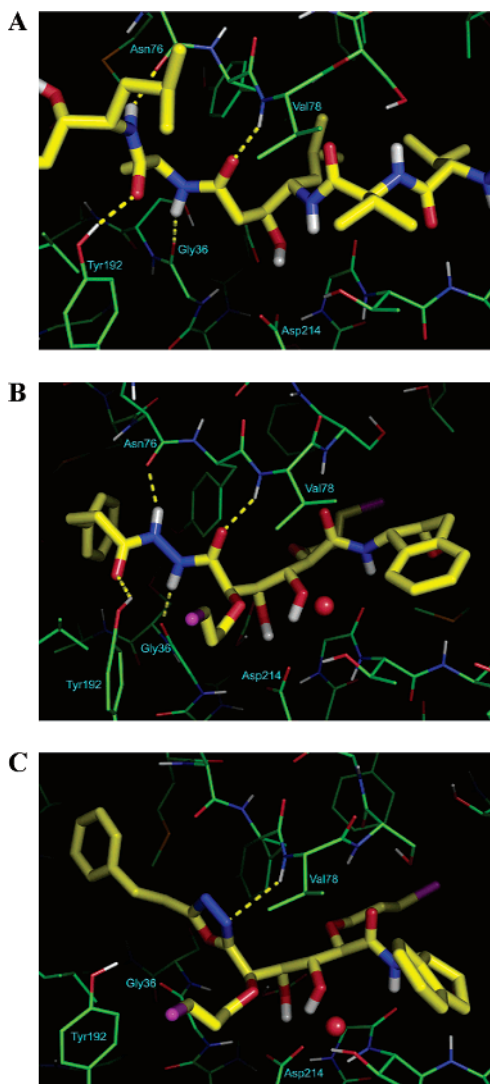


Figure 2. Comparison of H-bond network between Plm II and three ligands: (A) pepstatin A, (B) **9**, and (C) **23**. Plm II is shown in green and the ligands in yellow. Dashed yellow lines depict H-bonds, and it can be noted that the four H-bonds made with **9** matches the pattern of pepstatin A, while compound **23** loses several H-bonds and also has an unfavorable interaction between the carbonyl of Gly36 and the oxadiazole oxygen.

X-ray structures of Plm II complexes with ligands having large P2' groups (1LEE, 1LF2).³³

The ability of MD simulation to elicit the opening of the S2' pocket prompted us to also examine this conformation in combination with the other compounds. The other diacylhydrazine containing compounds **9**, **15** and **16**, also showed highly increased stability in the P2' region when the pocket was enlarged. The adopted conformation of the P2' group allows for strong H-bond interactions between the diacylhydrazine spacer and Gly36, Asn76, Val78 and Tyr192, as seen in Figure 2. The predicted binding conformation also allows the phenyl group of the ligand to reside in a predominantly hydrophobic environment in the S2' pocket formed by Met75, Tyr77, Leu131 and Ile133.

Compound **5** is similar to **9** but lacks the terminal benzyl group in P2', and the effect of this is that the hydrogen bonds between the diacylhydrazine and the protein are somewhat weakened. The phenyl moiety of **9** bound in S2' thus appears to stabilize the conforma-

tion required for these hydrogen bonds, and for **5** the terminal interaction with the hydroxyl of Tyr192 is completely lost.

The opposite binding direction was investigated as well for **5**, **9**, and **14–16**, i.e., with the diacylhydrazine linker on the nonprime side. The MD simulations show that the phenyl fragment cannot be fully accommodated in the S2 pocket and remains solvent exposed during these simulations where its conformation fluctuates substantially. In this binding mode the diacylhydrazine mainly interacts with H-bond donors/acceptors from the protein backbone, namely the Ser79 and Ser218 amide nitrogens and the carbonyl of Gly216, but these interactions are less stable due to the mobility of the phenyl group.

In compounds **19** and **23** the diacylhydrazine is replaced by the oxadiazole ring. Both the ring oxygen and the ring nitrogens may act as hydrogen bond acceptors, while no donor function is present in contrast to the diacylhydrazines. Compounds **19** and **23** did not show the same conformational stability during MD as the other compounds examined. In the orientation with the oxadiazole on the prime side, one of the two nitrogens in the ring makes an H-bond to the backbone nitrogen of Val78. The other nitrogen is exposed to solvent, and the oxygen is forced into an unfavorable orientation with respect to the Gly36 carbonyl group, which destabilizes the oxadiazole compared to the diacylhydrazine substituent. Furthermore the oxadiazole linker to the phenyl group is shorter in **23**, making it harder for the phenyl group to reach into the S2' pocket. When the oxadiazole instead is located on the nonprime side, the heterocyclic nitrogens form close interactions with the amide hydrogen of Ser79, forcing the ring oxygen to make unfavorable interactions with the carbonyl oxygen of Gly216 in a manner similar to the other conformation.

With the diacylhydrazine or heterocyclic fragment of the investigated ligands located to the prime side, the indanol group at the other end of the ligands is located in the S2 subsite. There it makes hydrophobic contact with the residues that form the S2 pocket, Val78, Thr217, Ala219, Ile290 and Ile292, as found earlier.²⁷ The hydroxyl group of the indanol can either hydrogen bond to the Ser218 side chain or make contact with the solution. In the mirrored conformation, the indanol is accommodated in S2', but does not stretch all the way to Met75 mentioned above. Instead it stays close to the flap and makes hydrophobic contact only to the flap residues Tyr77 and Val78, thereby leaving a large portion of the aliphatic indan ring solvent exposed. The hydroxyl group then fluctuates between interactions with the amide oxygen of Asn76 and an internal H-bond to the adjacent carbonyl in the ligand, as observed earlier.²⁷

Complementary docking of ligand **16** was performed with Autodock to investigate if the binding mode found here could be reproduced when the Met75 side chain was rotated manually in the Plm II structure. The rotation was made by shifting the torsion C β -C γ -S δ -C ϵ 180°, thus causing a substantial movement of the C ϵ atom resulting in an expansion of the S2' pocket. When docking was done with the 1SME¹⁹ structure with the side chain of Met75 rotated, we still found no

reasonable solutions. However, when the structure 1LF2³³ was used, where the S2' pocket is in the open conformation, several good solutions were found. Clustering the 150 independent solutions gave a small cluster of 2 and a larger of 22 with low docking energy score. The cluster with only 2 members had the diacylhydrazine in the nonprime position, and the larger cluster had the diacylhydrazine on the prime side. In the other structure denoted 1LF3,³⁹ the side chain of Met75 has the same conformation as in 1SME, i.e., S2' is closed, but the active site of PlmII is generally more open than in 1SME. Docking was also performed in 1LF3 without rotating the Met75 side chain. The outcome was clustered as earlier, resulting in 2 clusters of 29 and 18 solutions, respectively. Both clusters had the diacylhydrazine on the prime side differing essentially only in the position of the terminal phenyl group. When the Met75 side chain was rotated we found 3 clusters containing 36, 3 and 17 solutions, respectively. The cluster of 36 solutions had the diacylhydrazine spacer on the prime side, and so did the cluster of 17. The larger cluster of the two had only few solutions in which the phenyl was docked in the open S2', but in the latter a majority had the phenyl enclosed by the S2'. The small cluster of three solutions had the opposite conformation, i.e., the diacylhydrazine was found in the nonprime position. These calculations thus further support the conformations found by MD, but also illustrate how automated rigid-receptor docking can be sensitive to protein conformation, especially when binding pockets are partially collapsed.

Discussion

We have previously identified highly potent inhibitors of Plm I and II comprising a C₂-symmetric 1,2-dihydroxyethylene scaffold.^{26,27} With respect to the direction of the P2 and P2' side chains in these inhibitors (**1** and **2**),²⁷ as deduced from molecular modeling a diacylhydrazine element (**3–16**) or a 1,3,4-oxadiazole (**17–24**) should constitute proper amide bond replacements. The effect of replacing the amino indanols, previously employed both as P2 and P2' side chains, were simultaneously examined. As demonstrated in Table 1, several potent inhibitors of both Plm I and II with K_i values in the low nanomolar range were identified (**9–11** and **14**). The symmetrical compounds (**3** and **4**, and **17** and **18**), in which both of the amide bonds in the backbone as well as the indanol had been replaced, were generally significantly less active in the Plm I and II assays as compared to the unsymmetrical variants.

With the introduced asymmetry in the P2/P2' positions, predictions regarding possible binding modes of the new substituents are important to further ligand development. Automated docking, as a tool for determining binding modes, is less reliable when a high degree of torsional freedom is present in the ligands, especially in combination with a flexible receptor as Plm II. As previously, we attempted to overcome this problem by using MD to examine the binding of the new ligands to Plm II.^{26,27} The average structures obtained from the simulations did not offer any differences regarding the central parts of the ligands (the two central hydroxyls and the P1/P1' groups) from the earlier studies on symmetrical inhibitors.^{26,27} However,

the obtained binding directions of the two new amide replacements provided more detailed predictions regarding structure–activity relationships for these types of compounds.

For all of the unsymmetrical inhibitors, the most favorable binding direction predicted by the MD simulations was with the diacylhydrazine/oxadiazole spacer on the prime side rather than on the nonprime side, as depicted in Chart 1. In practically all cases polar interactions were more favorable for this pose than the reverse one. For compounds with larger P2' substituents, the capability of S2' to open up a large hydrophobic pocket appears essential for accommodating this binding mode, as illustrated in Figure 1. The flexibility in S2' mainly arises from different conformations of the Met75 side chain, and the ability of MD simulations to capture the opening of S2' is a pertinent example of induced fit between ligand and receptor. Furthermore, it is quite remarkable how well the protein can adopt to this large phenethyl P2' group by essentially only one conformational change of a single side chain. The predicted protein conformational change is also supported by experimental data on the complex of Plm II with the inhibitor rs370, where a bulky 4-aminophenyl P2' substituent occupies the same space as the phenyl group.³³ Both the calculated binding affinities and complementary docking predicted the same favored binding mode. The diacylhydrazine element is able to establish a rigid hydrogen bond network involving the backbone of Gly36, Asn76, Val78 and the Tyr192 side chain in the active site of Plm II, which mimics the network formed by pepstatin A in complex with Plm II (Figure 2). It is reasonable to expect that such an H-bond pattern also occur with the natural peptide substrate. The heterocyclic oxadiazole in compound **23** functions as a shorter linker to the phenyl group in the P2/P2' position than the diacylhydrazine linker. Even with an extra carbon atom, as in the phenylpropyl chain of **24**, the phenyl ring is not likely to be as stable as in the diacylhydrazine case since the oxadiazole is found to be unable to make the rigid H-bond pattern observed with the diacylhydrazine. Even if **19** and **23** are less potent inhibitors the calculated binding affinities for **19** and **23** still favor the binding mode with the oxadiazole on the prime side, consistent with the diacylhydrazine compounds. The affinity difference between the oxadiazole and diacylhydrazine inhibitors can best be understood by comparing **5** and **19** where the only difference is the amide bond replacement. Analysis of the difference in nonbonded interactions in **5** and **19** (Figure 3) clearly shows that the largest difference involves an unfavorable interaction of the oxadiazole oxygen of **19** with the carbonyl oxygen of Gly36 while the diacylhydrazine in **5** forms a hydrogen bond with the same Gly36 carbonyl.

The somewhat overpredicted affinity for **15** (K_i^{calc} = 12 vs K_i^{expt} = 145 nM) was found to originate from a hydrophobic collapse of the ligand in the simulated unbound state. This phenomenon was examined in an additional simulation of **15** employing ligand restraints in water to prevent hydrophobic collapse, and the corresponding results (K_i^{calc} = 50 nM) show better agreement with experimental result. The only term affected in the water simulation turns out to be the

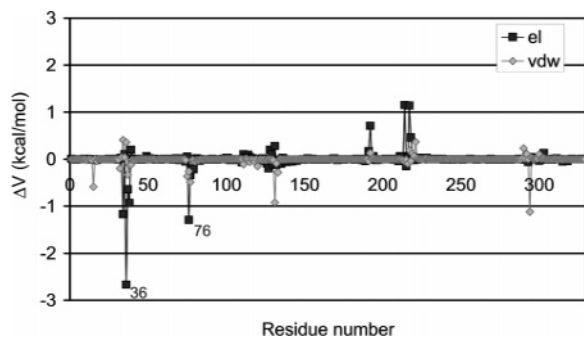


Figure 3. Plot of the difference in average nonbonded interactions between compound **5** and **19** to each Plm II residue (a negative value corresponds to stronger interactions of ligand **5** with the specific amino acid). The interactions are averaged over 1 ns and separated into van der Waals and electrostatic terms. The negative electrostatic value for Gly36 clearly shows the more favorable interaction (H-bond) of **5**, which in the case of **19** is replaced by an oxygen–oxygen repulsion.

nonpolar one, while the electrostatic contribution is unaffected by the restraints. When similar restraints were applied to other ligands, the effect on the energetics was insignificant. We therefore suspect that the observed hydrophobic collapse may be related to the recently reported finding that several current force fields, including the one used here, has slightly too favorable nonpolar interactions.^{49,50} This overstabilizes the “folded” state of peptide- or polymer-like molecules and, in reality, the tendency to start packing hydrophobic groups should probably occur somewhat later on the molecular size-scale.

Within the unsymmetrical diacylhydrazine series of bis(vinyl bromides) (**5**–**13**), inhibitors with higher affinity to both Plm I and II compared to the parent compound **2** were encountered (e.g. **9**, **10**, and **11**). Unfortunately, an extension of the P1 and P1' side chain did not result in the same increase in activity as previously reported for the C₂-symmetrical diamides.

Notably, in the Plm IV assay the opposite relative activity between the oxadiazole and the diacylhydrazine series was observed, based on the activities of two inhibitors (**4** and **18**). The 1,3,4-oxadiazole **18** demonstrated a significantly higher inhibitory activity than the diacylhydrazine **4**. Whether this behavior is due to the different nature of the flap loop in the two proteins, with the more flexible Gly in Plm IV instead of the Val at position 78 of Plm II, is currently being investigated by computational methods. The fact that, the oxadiazole **18** that is Plm IV selective and displayed inhibition of parasite growth in cell culture suggests that other plasmepsins than Plm I/Plm II might be essential for the parasite replication, as has previously been proposed.^{13,51,52} In fact Plm IV is the ortholog of the only food vacuole plasmepsin found in the three remaining human *Plasmodium* species, *P. vivax*, *P. malaria*, and *P. ovale*, making it a potential target for multi species antimalarials.^{13,52} In this context, it is important to emphasize that recent studies of *P. falciparum* plasmepsin knock-out clones implies the significance of inhibiting several of the food vacuole plasmepsins in order to efficiently kill the parasite.^{53,54}

Conclusion

Potent Plm I and II inhibitors derived from L-mannitol and characterized by either a diacylhydrazine or a five-membered oxadiazole ring replacing the prime side amide have been designed and synthesized. MD simulations were applied in the design process. The computationally predicted Plm II K_i values were generally in excellent agreement with the biological results and the predicted bioactive conformations were supported by crystal structures of other inhibitors. The diacylhydrazine was found to be superior over the oxadiazole as amide bond replacement in Plm I and II inhibitors. According to the computationally predicted conformation this was primarily attributed to the diacylhydrazine being able to form an extensive hydrogen bond network, similar to pepstatin A, to the active site. Moreover, an extensive flexibility of the S2' pocket was captured by the simulations, predicting the binding mode of the unsymmetrical inhibitors to be with the amide bond replacement orientated to the prime side, as illustrated in Chart 1.

All inhibitors prepared display a unique selectivity over the human Cat D. One of the symmetrical compounds with both of the two amide bonds replaced by oxadiazole rings was found to be strongly active toward Plm IV. This Plm IV selective compound (**18**) was also effective in culture inhibiting infected erythrocytes and could possibly serve as a lead for further optimization. Actually, this inhibitor, although with a relatively high molecular weight (Mw 760), was totally devoid of amide bonds and represents, to the best of our knowledge, the so far most potent nonpeptidic inhibitor of Plm IV disclosed (K_i = 35 nM).

Experimental Section

Chemistry. General Information. All microwave reactions were conducted in heavy-walled glass Smith process vials sealed with aluminum crimp caps fitted with a silicon septum. The microwave heating was performed in a Smith Synthesizer single-mode microwave cavity producing continuous irradiation at 2450 MHz (Biotage AB, Uppsala, Sweden). Reaction mixtures were stirred with a magnetic stirring bar during the irradiation. The temperature, pressure and irradiation power were monitored during the course of the reaction. After completed irradiation, the reaction tube was cooled with high-pressure air until the temperature had fallen below 39 °C. The hydrazides used for the synthesis of the compounds **3**–**8** and **11** were purchased from Sigma-Aldrich. ¹H and ¹³C NMR spectra were recorded on a JEOL JNM-EX 270 spectrometer at 270.2 and 67.8 MHz, respectively or on a JEOL JNM-EX400 spectrometer at 399.8 and 100.5 MHz, respectively. HMBC and HSQC spectra were recorded on a Varian UNITY INOVA spectrometer (¹H at 499.9 MHz). Chemical shifts are reported as δ values (ppm) indirectly referenced to TMS via the solvent residual signal. Optical rotations were obtained on a Perkin-Elmer 241 polarimeter. Specific rotations ($[\alpha]_D$) are reported in deg/dm, and the concentration (*c*) is given in g/100 mL in the specified solvent. Elemental analyses were performed by Analytische Laboratorien, Lindlar, Germany. Flash column chromatography was performed on Merck silica gel 60, 0.04–0.063 mm. Thin-layer chromatography was performed using aluminum sheets precoated with silica gel 60 F₂₅₄ (0.2 mm; E. Merck, eluent 0–10% MeOH in CHCl₃) and visualized with UV light and ninhydrin. Analytical RP-LC-MS was performed on a Gilson HPLC system with a Chromolith Performance RP-18e 100 × 4.6 mm (Merck KGaA) column, with a Finnigan AQA quadrupole mass spectrometer, at a flow rate of 4 mL/min, using different gradients of CH₃CN in 0.05% aqueous

formic acid. Preparative RP-LC-MS was performed on Gilson HPLC system with a Zorbax SB-C8, 5 μ m 21.2 \times 150 mm (Agilent Technologies) column, with a Finnigan AQA quadrupole mass spectrometer, at a flow rate of 15 mL/min.

(2R)-1N-(2-Hydroxyindan-1-yl)-2-(2-propenyloxy)-2-[(2R,3R,4R)-4-(2-propenyloxy)-3-hydroxy-5-oxo-tetrahydrofuran-2-yl]-ethanamide (28). The bislactone **26** (78 mg, 0.31 mmol) and 2-hydroxypyridine (29 mg, 0.30 mmol) were dissolved in dry CH₂Cl₂ (5 mL) and stirred at room temperature for 30 min. The solution was cooled to 0 °C, and (1S,2R)-1-amino-2-indanol (46 mg, 0.31 mmol) was added rapidly. The reaction mixture was allowed to attain room temperature and stirred overnight for 17 h. The reaction was monitored by TLC and analytical RP-LC-MS. The solvent was removed under reduced pressure, and subsequent purification by flash chromatography (CHCl₃) gave **28** (52 mg, 42%) as a white solid: $[\alpha]^{20}_D -31.0^\circ$ ($c = 1.00$, CH₃CN). Anal. (C₂₁H₂₅NO₇) C, H, N.

(2R)-2-[(2E)-3-Bromo-2-propenyloxy]-2-[(2R,3R,4R)-4-(2E)-3-bromo-2-propenyloxy]-3-hydroxy-5-oxo-tetrahydrofuran-2-yl]-1N-(2-hydroxyindan-1-yl)-ethanamide (29). The bislactone **27** (400 mg, 0.97 mmol) and 2-hydroxypyridine (92 mg, 0.97 mmol) were dissolved in dry CH₂Cl₂ (20 mL) and stirred at room temperature for 30 min. The solution was cooled to 0 °C, and (1S,2R)-1-amino-2-indanol (144 mg, 0.97 mmol) was added rapidly. The reaction mixture was allowed to attain room temperature and stirred overnight for 15 h. The reaction was monitored by TLC and analytical RP-LC-MS. The solvent was removed under reduced pressure, and subsequent purification by flash chromatography (CHCl₃) gave **29** (238 mg, 44%) as a white solid: $[\alpha]^{23}_D -17.0^\circ$ ($c = 1.06$, CH₃CN). Anal. (C₂₁H₂₃Br₂NO₇) C, H, N.

(2R,3R,4R,5R)-2,5-Bis[(2E)-3-bromo-2-propenyloxy]-1,6-(N'-ethanoylhydrazino)-3,4-dihydroxyhexan-1,6-dione (3). Bislactone **27** (100 mg, 0.24 mmol) and acetic hydrazide (130 mg, 1.8 mmol) were dissolved in dry CH₂Cl₂ (5 mL), and the reaction mixture was stirred at reflux for 56 h. The reaction was monitored by TLC and analytical RP-LC-MS. The solvent was removed under reduced pressure, and subsequent purification by flash chromatography (3–10% MeOH in CHCl₃) gave **3** (41 mg, 30%) as a white solid: $[\alpha]^{23}_D +36.2^\circ$ ($c = 0.82$, MeOH). Anal. (C₁₆H₂₄Br₂N₄O₈) C, H, N.

(2R,3R,4R,5R)-2,5-Bis[(2E)-3-bromo-2-propenyloxy]-1,6-Bis[N'-(4-tert-butylbenzoyl)hydrazino]-3,4-dihydroxyhexan-1,6-dione (4). Bislactone **27** (50 mg, 0.12 mmol) and 4-tert-butylbenzoyl hydrazide (165 mg, 0.86 mmol) were dissolved in dry CH₂Cl₂ (3 mL), and the reaction mixture was stirred at reflux for 64 h. The reaction was monitored by TLC and RP-LC-MS. The solvent was removed under reduced pressure, and subsequent purification by flash chromatography (0–6% MeOH in CHCl₃) gave **4** (67 mg, 70%) as a white solid: $[\alpha]^{23}_D +35.2^\circ$ ($c = 0.49$, MeOH). Anal. (C₃₄H₄₄Br₂N₄O₈) C, H, N.

General Procedure I. Synthesis of the Unsymmetrical Diacylhydrazines 5–13 and 16. A mixture of the monolactone and hydrazide was refluxed in dry CH₂Cl₂ (17–47 h). The reaction was monitored by TLC and analytical RP-LC-MS. Purification as indicated gave **5–13** and **16**.

(2R,3R,4R,5R)-2,5-Bis[(2E)-3-bromo-2-propenyloxy]-6-(N'-ethanoylhydrazino)-3,4-dihydroxy-N1-[(1S,2R)-2-hydroxyindan-1-yl]-6-oxo-hexanamide (5). Compound **5** was prepared according to general procedure I using monolactone **29** (85 mg, 0.15 mmol) and acetic hydrazide (115 mg, 1.6 mmol) dissolved in CH₂Cl₂ (2 mL). Purification by flash chromatography (0–10% MeOH in CHCl₃) gave **5** (61 mg, 64%) as a white solid: $[\alpha]^{23}_D +35.8^\circ$ ($c = 0.34$, MeOH). Anal. (C₂₃H₂₉Br₂N₃O₈) C, H, N.

(2R,3R,4R,5R)-6-(N'-Benzoylhydrazino)-2,5-Bis[(2E)-3-bromo-2-propenyloxy]-3,4-dihydroxy-N1-[(1S,2R)-2-hydroxyindan-1-yl]-6-oxo-hexanamide (6). Compound **6** was prepared according to general procedure I using monolactone **29** (85 mg, 0.15 mmol) and benzoic hydrazide (209 mg, 1.5 mmol) dissolved in CH₂Cl₂ (2 mL). Purification by flash chromatography (2–8% MeOH in CHCl₃) gave **6** (74 mg, 71%)

as a white solid: $[\alpha]^{23}_D +39.0^\circ$ ($c = 0.96$, MeOH). Anal. (C₂₈H₃₁Br₂N₃O₈) C, H, N.

(2R,3R,4R,5R)-2,5-Bis[(2E)-3-bromo-2-propenyloxy]-6-[N'-(4-tert-butylbenzoyl)hydrazino]-3,4-dihydroxy-N1-[(1S,2R)-2-hydroxyindan-1-yl]-6-oxo-hexanamide (7). Compound **7** was prepared according to general procedure I using monolactone **29** (39 mg, 0.070 mmol) and 4-tert-butylbenzoic hydrazide (69 mg, 0.36 mmol) dissolved in CH₂Cl₂ (1.5 mL). Purification by flash chromatography (0–10% MeOH in CHCl₃) and RP-LC-MS (30 min gradient of 30–70% CH₃CN in 0.05% aqueous formic acid) gave **7** (36 mg, 69%) as a white solid: $[\alpha]^{23}_D +9.2^\circ$ ($c = 1.14$, CHCl₃). Anal. (C₃₂H₃₉Br₂N₃O₈) C, H, N.

(2R,3R,4R,5R)-2,5-Bis[(2E)-3-bromo-2-propenyloxy]-3,4-dihydroxy-N1-[(1S,2R)-2-hydroxyindan-1-yl]-6-oxo-6-[N'-(2-phenylethanoyl)hydrazino]-hexanamide (8). Compound **8** was prepared according to general procedure I using monolactone **29** (95 mg, 0.17 mmol) and phenylacetic hydrazide (255 mg, 1.7 mmol) dissolved in CH₂Cl₂ (2 mL). Purification by flash chromatography (0–6% MeOH in CHCl₃) gave **8** (92 mg, 76%) as a white solid: $[\alpha]^{23}_D +30.1^\circ$ ($c = 1.25$, MeOH); Anal. (C₂₉H₃₃Br₂N₃O₈) C, H, N.

(2R,3R,4R,5R)-2,5-Bis[(2E)-3-bromo-2-propenyloxy]-3,4-dihydroxy-N1-[(1S,2R)-2-hydroxyindan-1-yl]-6-oxo-6-[N'-(3-phenylpropanoyl)hydrazino]-hexanamide (9). Compound **9** was prepared according to general procedure I using monolactone **29** (100 mg, 0.18 mmol) and 3-phenyl-propionic acid hydrazide (prepared according to literature procedure,⁵⁵ 246 mg, 1.5 mmol) dissolved in CH₂Cl₂ (3 mL). Purification by flash chromatography (2–5% MeOH in CHCl₃) gave **9** (96 mg, 74%) as a white solid: $[\alpha]^{23}_D +33.3^\circ$ ($c = 0.87$, MeOH). Anal. (C₃₀H₃₅Br₂N₃O₈) C, H, N.

(2R,3R,4R,5R)-2,5-Bis[(2E)-3-bromo-2-propenyloxy]-3,4-dihydroxy-N1-[(1S,2R)-2-hydroxyindan-1-yl]-6-oxo-6-[N'-(4-phenylbutanoyl)hydrazino]-hexanamide (10). Compound **10** was prepared according to general procedure I using monolactone **29** (99 mg, 0.18 mmol) and 4-phenylbutyric acid hydrazide (prepared according to literature procedure,⁵⁵ 301 mg, 1.7 mmol) dissolved in CH₂Cl₂ (2 mL). Purification by flash chromatography (0–5% MeOH in CHCl₃) gave **10** (98 mg, 74%) as a white solid: $[\alpha]^{20}_D +30.3^\circ$ ($c = 1.00$, MeOH). Anal. (C₃₁H₃₇Br₂N₃O₈) C, H, N.

(2R,3R,4R,5R)-2,5-Bis[(2E)-3-bromo-2-propenyloxy]-3,4-dihydroxy-N1-[(1S,2R)-2-hydroxyindan-1-yl]-6-[N'-(3-1H-indol-3-yl-propanoyl)hydrazino]-6-oxo-hexanamide (11). Compound **11** was prepared according to general procedure I using monolactone **29** (65 mg, 0.12 mmol) and 3-indolepropionic acid hydrazide (237 mg, 1.2 mmol) dissolved in CH₂Cl₂ (1 mL). Purification by flash chromatography (0–10% MeOH in CHCl₃) gave **11** (45 mg, 51%) as a white solid: $[\alpha]^{20}_D +31.5^\circ$ ($c = 0.99$, MeOH). Anal. (C₃₂H₃₆Br₂N₄O₈) C, H, N.

(2R,3R,4R,5R)-2,5-Bis[(2E)-3-bromo-2-propenyloxy]-3,4-dihydroxy-N1-[(1S,2R)-2-hydroxyindan-1-yl]-6-[N'-(3-morpholin-4-yl-propanoyl)hydrazino]-6-oxo-hexanamide (12). Compound **12** was prepared according to general procedure I using monolactone **29** (30 mg, 0.053 mmol) and 3-(morpholin-4-yl)propionic acid hydrazide (prepared according to literature procedure,⁵⁶ 93 mg, 0.54 mmol) dissolved in CH₂Cl₂ (0.8 mL). Purification by RP-LC-MS (30 min gradient of 5–50% CH₃CN in 0.05% aqueous formic acid), filtration through basic aluminum oxide 90 (0.063–0.2 mm; E. Merck) and flash chromatography (3–10% MeOH in CHCl₃) gave **12** (18 mg, 45%) as a white solid: $[\alpha]^{18}_D +28.3^\circ$ ($c = 0.91$, MeOH). Anal. (C₂₈H₃₈Br₂N₄O₉) C, H, N.

(2R,3R,4R,5R)-2,5-Bis[(2E)-3-bromo-2-propenyloxy]-3,4-dihydroxy-N1-[(1S,2R)-2-hydroxyindan-1-yl]-6-oxo-6-[N'-(3-(4-methylpiperazin-1-yl)-propanoyl)hydrazine]-hexanamide dihydrochloride (13). Compound **13** was prepared according to general procedure I using monolactone **29** (35 mg, 0.062 mmol) and 3-(4-methylpiperazin-1-yl)propionic acid hydrazide (prepared according to literature procedure,⁵⁷ 100 mg, 0.54 mmol) dissolved in CH₂Cl₂ (0.8 mL). Purification by RP-LC-MS (30 min gradient of 0–55% CH₃CN in 0.05% aqueous formic acid) gave **13** (11 mg, 22%) as

the formate salt. A small portion was transformed to the dihydrochloride salt and analyzed: $[\alpha]^{20}_D +19.9^\circ$ ($c = 0.47$, MeOH). Anal. ($C_{25}H_{43}Br_2Cl_2N_5O_8$) C, H, N.

(2R,3R,4R,5R)-2,5-Bis(2-propenyloxy)-3,4-dihydroxy-N1-[(1S,2R)-2-hydroxyindan-1-yl]-6-oxo-6-[N'-(3-phenylpropanoyl)hydrazino]-hexanamide (16). Compound **16** was prepared according to general procedure I using monolactone **28** (51 mg, 0.13 mmol) and 3-phenyl-propionic acid hydrazide (prepared according to literature procedure,⁵⁵ 210 mg, 1.3 mmol) dissolved in CH_2Cl_2 (1.5 mL). Purification by flash chromatography (0–4% MeOH in $CHCl_3$) gave **16** (53 mg, 74%) as a white solid: $[\alpha]^{21}_D +45.9^\circ$ ($c = 1.02$, MeOH). Anal. ($C_{30}H_{37}N_3O_8$) C, H, N.

(1R,2R,3R,4R)-1,4-Bis[(2E)-3-bromo-2-propenyloxy]-1,4-bis(5-methyl-[1,3,4]oxadiazol-2-yl)-butane-2,3-diol (17). To a stirred solution of diacyl hydrazine **3** (75 mg, 0.13 mmol) in dry CH_2Cl_2/THF 1:1 (6 mL) were added chlorotrimethylsilane (510 μ L, 4.0 mmol) and triethylamine (650 μ L, 4.7 mmol). Since the reaction was slow, additional amounts of chlorotrimethylsilane (510 μ L, 4.0 mmol after 2 h) and triethylamine (650 μ L, 4.7 mmol after 2 h) were added. The reaction mixture was stirred at room temperature for 19 h, and the reaction was monitored by TLC and analytical RP-LC-MS. The solvent was removed under reduced pressure, and subsequent purification by flash chromatography (0–0.5% MeOH in $CHCl_3$) gave the TMS-protected diacyl hydrazine (51 mg, 56%) as a white solid: $[\alpha]^{23}_D -89.4^\circ$ ($c = 1.04$, $CHCl_3$). Anal. ($C_{22}H_{40}Br_2N_4O_8Si_2$) C, H, N.

TMS-protected diacyl hydrazine (51 mg, 0.072 mmol) and Burgess reagent (104 mg, 0.44 mmol) were dissolved in dry THF (0.5 mL), and the reaction mixture was stirred at reflux for 3 h. The reaction was monitored by analytical RP-LC-MS. The solvent was removed under reduced pressure, and the residue was partitioned between $CHCl_3$ (10 mL) and H_2O (10 mL). The aqueous layer was extracted with $CHCl_3$ (2×10 mL), and the combined organic layers were washed with H_2O (30 mL), dried (Na_2SO_4) and concentrated. The crude product and $KF \cdot 2H_2O$ (400 mg, 4.2 mmol) were dissolved in MeOH (3 mL), and stirred at room temperature for 18 h. The reaction was monitored by analytical RP-LC-MS. The solvent was removed under reduced pressure and the residue was partitioned between $CHCl_3$ (30 mL) and brine (30 mL). The aqueous layer was extracted with $CHCl_3$ (2×30 mL) and the combined organic layers were washed with H_2O (30 mL), dried (Na_2SO_4), and concentrated. Purification by flash chromatography (0–4% MeOH in $CHCl_3$) gave **17** (10 mg, 27%) as a white solid: $[\alpha]^{23}_D +56.6^\circ$ ($c = 1.03$, $CHCl_3$). Anal. ($C_{16}H_{20}Br_2N_4O_6$) C, H, N.

(1R,2R,3R,4R)-1,4-Bis[(2E)-3-bromo-2-propenyloxy]-1,4-bis[5-(4-tert-butylphenyl)-[1,3,4]oxadiazol-2-yl]-butane-2,3-diol (18). To a stirred solution of diacyl hydrazine **4** (49 mg, 0.061 mmol) in dry CH_2Cl_2 (3 mL) were added chlorotrimethylsilane (150 μ L, 1.2 mmol) and triethylamine (190 μ L, 1.4 mmol). Since the reaction was slow, additional amounts of chlorotrimethylsilane (150 μ L, 1.2 mmol and 200 μ L, 1.6 mmol after 4 and 22 h, respectively) and triethylamine (250 μ L, 1.8 mmol and 250, 1.8 mmol after 4 and 22 h, respectively) were added. The reaction mixture was stirred at room temperature for 48 h. The reaction was monitored by TLC and analytical RP-LC-MS. The solvent was removed under reduced pressure, and subsequent purification by flash chromatography (pentane/ $CHCl_3$ /MeOH, 60:40:1) gave the TMS-protected diacyl hydrazine (48 mg, 83%) as a white solid: $[\alpha]^{23}_D -34.1^\circ$ ($c = 1.00$, $CHCl_3$). Anal. ($C_{40}H_{60}Br_2N_4O_8Si_2$) C, H, N.

TMS-protected diacyl hydrazine (49 mg, 0.052 mmol) and Burgess reagent (188 mg, 0.79 mmol) were dissolved in dry THF (3 mL). Since the reaction was slow, an additional amount of Burgess reagent (70 mg, 0.29 mmol and 187 mg, 0.78 mmol after 2 and 3 h, respectively) was added. The reaction mixture was stirred at reflux for 4 h. The reaction was monitored by analytical RP-LC-MS. The solvent was removed under reduced pressure, and the residue was dissolved in $CHCl_3$, filtered through a pad of silica (3 cm) and concentrated. The crude product and $KF \cdot 2H_2O$ (700 mg, 7.4 mmol) was dissolved in

MeOH (5 mL) and stirred at room temperature for 18 h. The reaction was monitored by analytical RP-LC-MS. The solvent was removed under reduced pressure, and the residue was partitioned between $CHCl_3$ (6 mL) and H_2O (6 mL). The aqueous layer was extracted with $CHCl_3$ (2×6 mL), and the combined organic layers were dried (Na_2SO_4), and concentrated. Purification by RP-LC-MS (30 min gradient of 90–100% CH_3CN in 0.05% aqueous formic acid) gave **18** (23 mg, 58%) as a white solid: $[\alpha]^{23}_D +81.1^\circ$ ($c = 0.88$, $CHCl_3$). Anal. ($C_{34}H_{40}Br_2N_4O_6$) C, H, N.

General Procedure II. Synthesis of the Unsymmetrical 1,3,4-Oxadiazoles 19–24. A mixture of the diacylhydrazine, chlorotrimethylsilane, and triethylamine in dry CH_2Cl_2 was stirred at room temperature (16–28h). The reaction was monitored by TLC and analytical RP-LC-MS. Purification as indicated gave the TMS-protected diacylhydrazine.

In the subsequent cyclization TMS-protected diacylhydrazine and Burgess reagent in dry THF were stirred at reflux (4–6 h). The reaction was monitored with analytical RP-LC-MS. The solvent was removed under reduced pressure, and the crude product was (if nothing else is indicated) deprotected without further purification. The crude product and $KF \cdot 2H_2O$ were dissolved in MeOH and stirred at room temperature (14–22h). The reaction was monitored with RP-LC-MS. Purification as indicated gave **19–24**.

(2R,3R,4R,5R)-2,5-Bis[(2E)-3-bromo-2-propenyloxy]-3,4-dihydroxy-N1-[(1S,2R)-2-hydroxyindan-1-yl]-5-(5-methyl-[1,3,4]oxadiazol-2-yl)-pentanamide (19). Protection of the diacylhydrazine **5** (49 mg, 0.077 mmol) was accomplished according to general procedure II using chlorotrimethylsilane (490 μ L, 3.9 mmol) and triethylamine (560 μ L, 4.0 mmol) dissolved in dry CH_2Cl_2 (3 mL). Purification by flash chromatography ($CHCl_3$) gave the TMS-protected diacyl hydrazine (62 mg, 95%) as a white solid: $[\alpha]^{24}_D +35.7^\circ$ ($c = 0.90$, $CHCl_3$). Anal. ($C_{32}H_{53}Br_2N_3O_8Si_3$) C, H, N.

The subsequent cyclization was carried out essentially according to general procedure II using the TMS-protected diacyl hydrazine (77 mg, 0.090 mmol) and Burgess reagent (86 mg, 0.36 mmol) dissolved in dry THF (0.5 mL). Since the reaction was slow, an additional amount of Burgess reagent (30 mg, 0.13 mmol after 3 h) was added. In the deprotection of the crude product $KF \cdot 2H_2O$ (500 mg, 5.3 mmol) and MeOH (3 mL) was used. The solvent was removed under reduced pressure, and the residue was partitioned between $CHCl_3$ (10 mL) and brine (10 mL). The aqueous layer was extracted with $CHCl_3$ (3×10 mL), and the combined organic layers were dried (Na_2SO_4) and concentrated. Purification by RP-LC-MS (30 min gradient of 20–65% CH_3CN in 0.05% aqueous formic acid) gave **19** (12 mg, 21%) as a white solid: $[\alpha]^{23}_D +44.4^\circ$ ($c = 1.15$, MeOH). Anal. ($C_{23}H_{27}Br_2N_3O_7$) C, H, N.

(2R,3R,4R,5R)-2,5-Bis[(2E)-3-bromo-2-propenyloxy]-3,4-dihydroxy-N1-[(1S,2R)-2-hydroxyindan-1-yl]-5-(5-phenyl-[1,3,4]oxadiazol-2-yl)-pentanamide (20). Protection of the diacylhydrazine **6** (100 mg, 0.14 mmol) was accomplished according to general procedure II using chlorotrimethylsilane (910 μ L, 7.2 mmol) and triethylamine (1.0 mL, 7.5 mmol) dissolved in dry CH_2Cl_2 (5 mL). Purification by flash chromatography (0–0.5% MeOH in $CHCl_3$) gave the TMS-protected diacyl hydrazine (113 mg, 88%) as a white solid: $[\alpha]^{24}_D +27.5^\circ$ ($c = 0.97$, $CHCl_3$). Anal. ($C_{37}H_{55}Br_2N_3O_8Si_3$) C, H, N.

The subsequent cyclization was carried out according to general procedure II using the TMS-protected diacyl hydrazine (109 mg, 0.12 mmol) and Burgess reagent (86 mg, 0.36 mmol) dissolved in dry THF (0.8 mL). In the deprotection of the crude product $KF \cdot 2H_2O$ (650 mg, 6.9 mmol) and MeOH (5 mL) was used. The solvent was removed under reduced pressure, and the residue was partitioned between $CHCl_3$ (20 mL) and H_2O (20 mL). The aqueous layer was extracted with $CHCl_3$ (3×20 mL), and the combined organic layers were dried (Na_2SO_4) and concentrated. Purification by flash chromatography (1–2% MeOH in $CHCl_3$) gave **20** (64 mg, 79%) as a white solid: $[\alpha]^{20}_D +48.8^\circ$ ($c = 0.91$, MeOH). Anal. ($C_{28}H_{29}Br_2N_3O_7$) C, H, N.

(2R,3R,4R,5R)-2,5-Bis[(2E)-3-bromo-2-propenyloxy]-5-[5-(4-tert-butylphenyl)-[1,3,4]oxadiazol-2-yl]-3,4-dihydroxy-N1-[(1S,2R)-2-hydroxyindan-1-yl]-pentanamide (21). Protection of the diacyl hydrazine **7** (66 mg, 0.087 mmol) was accomplished according to general procedure II using chlorotrimethylsilane (1.1 mL, 8.7 mmol) and triethylamine (1.2 mL, 8.6 mmol) dissolved in dry CH₂Cl₂ (6 mL). Purification by flash chromatography (CHCl₃) gave the TMS-protected diacyl hydrazine (78 mg, 92%) as a white solid: [α]_D²⁴ +26.7° (*c* = 1.04, CHCl₃). Anal. (C₄₁H₆₃Br₂N₃O₈Si₃) C, H, N.

The subsequent cyclization was carried out essentially according to general procedure II using the TMS-protected diacyl hydrazine (78 mg, 0.080 mmol) and Burgess reagent (57 mg, 0.24 mmol) dissolved in dry THF (0.7 mL). Since the reaction was slow, an additional amount of Burgess reagent (20 mg, 0.084 mmol after 4 h) was added. The solvent was removed under reduced pressure, and the residue was partitioned between CHCl₃ (10 mL) and H₂O (10 mL). The aqueous layer was extracted with CHCl₃ (3 × 10 mL), and the combined organic layers were dried (Na₂SO₄) and concentrated. In the deprotection of the crude product KF·2H₂O (450 mg, 4.8 mmol) and MeOH (4 mL) was used. The solvent was removed under reduced pressure, and the residue was partitioned between CHCl₃ (10 mL) and H₂O (10 mL). The aqueous layer was extracted with CHCl₃ (3 × 10 mL), and the combined organic layers were dried (Na₂SO₄) and concentrated. Purification by flash chromatography (0–3% MeOH in CHCl₃) gave **21** (42 mg, 71%) as a white solid: [α]_D²² +50.5° (*c* = 1.22, CHCl₃). Anal. (C₃₂H₃₇Br₂N₃O₇) C, H, N.

(2R,3R,4R,5R)-5-(5-Benzyl-[1,3,4]oxadiazol-2-yl)-2,5-Bis[(2E)-3-bromo-2-propenyloxy]-3,4-dihydroxy-N1-[(1S,2R)-2-hydroxyindan-1-yl]-pentanamide (22). Protection of the diacyl hydrazine **8** (57 mg, 0.080 mmol) was accomplished according to general procedure II using chlorotrimethylsilane (510 μL, 4.0 mmol) and triethylamine (580 μL, 4.2 mmol) dissolved in dry CH₂Cl₂ (3 mL). Purification by flash chromatography (0–0.5% MeOH in CHCl₃) gave the TMS-protected diacyl hydrazine (63 mg, 85%) as a white solid: [α]_D¹⁹ +36.5° (*c* = 0.99, CHCl₃). Anal. (C₃₈H₅₇Br₂N₃O₈Si₃) C, H, N.

The subsequent cyclization was carried out according to general procedure II using the TMS-protected diacyl hydrazine (56 mg, 0.060 mmol) and Burgess reagent (58 mg, 0.24 mmol) dissolved in dry THF (0.5 mL). In the deprotection of the crude product KF·2H₂O (345 mg, 3.7 mmol) and MeOH (4 mL) was used. The solvent was removed under reduced pressure, and the residue was partitioned between CHCl₃ (10 mL) and H₂O (10 mL). The aqueous layer was extracted with CHCl₃ (3 × 10 mL), and the combined organic layers were dried (Na₂SO₄) and concentrated. Purification by flash chromatography (0–3% MeOH in CHCl₃) gave **22** (19 mg, 45%) as a white solid: [α]_D²⁰ +29.4° (*c* = 0.94, CHCl₃). Anal. (C₂₉H₃₁Br₂N₃O₇·1/2H₂O) C, H, N.

(2R,3R,4R,5R)-2,5-Bis[(2E)-3-bromo-2-propenyloxy]-3,4-dihydroxy-N1-[(1S,2R)-2-hydroxyindan-1-yl]-5-[5-(2-phenylethyl)-[1,3,4]oxadiazol-2-yl]-pentanamide (23). Protection of the diacyl hydrazine **9** (68 mg, 0.094 mmol) was accomplished according to general procedure II using chlorotrimethylsilane (570 μL, 4.5 mmol) and triethylamine (650 μL, 4.7 mmol) dissolved in dry CH₂Cl₂ (3.5 mL). Purification by flash chromatography (0–0.5% MeOH in CHCl₃) gave the TMS-protected diacyl hydrazine (78 mg, 88%) as a white solid: [α]_D²² +30.5° (*c* = 0.92, CHCl₃). Anal. (C₃₉H₅₉Br₂N₃O₈Si₃) C, H, N.

The subsequent cyclization was carried out according to general procedure II using the TMS-protected diacyl hydrazine (72 mg, 0.076 mmol) and Burgess reagent (56 mg, 0.23 mmol) dissolved in dry THF (0.5 mL). In the deprotection of the crude product KF·2H₂O (400 mg, 4.2 mmol) and MeOH (4 mL) was used. The solvent was removed under reduced pressure, and the residue was partitioned between CHCl₃ (20 mL) and H₂O (20 mL). The aqueous layer was extracted with CHCl₃ (3 × 20 mL), and the combined organic layers were dried (Na₂SO₄) and concentrated. Purification by flash chromatography (0–

2% MeOH in CHCl₃) gave **23** (25 mg, 47%) as a white solid: [α]_D²⁰ +33.1° (*c* = 0.92, MeOH). Anal. (C₃₀H₃₃Br₂N₃O₇) C, H, N.

(2R,3R,4R,5R)-2,5-Bis[(2E)-3-bromo-2-propenyloxy]-3,4-dihydroxy-N1-[(1S,2R)-2-hydroxyindan-1-yl]-5-[5-(2-phenylpropyl)-[1,3,4]oxadiazol-2-yl]-pentanamide (24). Protection of the diacyl hydrazine **10** (89 mg, 0.12 mmol) was accomplished according to general procedure II using chlorotrimethylsilane (760 μL, 6.0 mmol) and triethylamine 870 μL, 6.2 mmol) dissolved in dry CH₂Cl₂ (4.5 mL). Purification by flash chromatography (0–0.5% MeOH in CHCl₃) gave the TMS-protected diacyl hydrazine (82 mg, 72%) as a white solid: [α]_D¹⁹ +32.8° (*c* = 1.02, CHCl₃). Anal. (C₄₀H₆₁Br₂N₃O₈Si₃) C, H, N.

The subsequent cyclization was carried out according to general procedure II using the TMS-protected diacyl hydrazine (81 mg, 0.085 mmol) and Burgess reagent (60 mg, 0.25 mmol) dissolved in dry THF (0.6 mL). In the deprotection of the crude product KF·2H₂O (474 mg, 5.0 mmol) and MeOH (4 mL) was used. The solvent was removed under reduced pressure, and the residue was partitioned between CHCl₃ (20 mL) and H₂O (20 mL). The aqueous layer was extracted with CHCl₃ (3 × 20 mL), and the combined organic layers were dried (Na₂SO₄) and concentrated. Purification by flash chromatography (0–2% MeOH in CHCl₃) gave **24** (36 mg, 59%) as a white solid: [α]_D¹⁹ +32.9° (*c* = 1.01, CHCl₃). Anal. (C₃₁H₃₅Br₂N₃O₇) C, H, N.

(2R,3R,4R,5R)-2,5-Bis[(2E)-bromo-2-propenyloxy]-5-hydrazinocarbonyl-3,4-dihydroxy-N1-[(1S,2R)-2-hydroxyindan-1-yl]-pentanamide (30). The monolactone **29** (40 mg, 0.071 mmol) was suspended in EtOH (4 mL) and hydrazine hydrate (4.4 μL, 0.072 mmol) was added. After the addition the suspension clarified and after approximately 1 h the product started to precipitate. The reaction mixture was stirred at room temperature for 8 h. The reaction was monitored by TLC and analytical RP-LC-MS. The precipitated product was filtered off and washed with EtOH. Additional product was provided by flash chromatography (5–10% MeOH in CHCl₃) of the filtrate to give **30** (in a total of 36 mg, 85%) as white crystals: [α]_D²³ +31.2° (*c* = 1.10, MeOH). Anal. (C₂₁H₂₇Br₂N₃O₇) C, H, N.

(2R,3R,4R,5R)-2,5-Bis[(2E)-3-bromo-2-propenyloxy]-3,4-dihydroxy-N1-[(1S,2R)-2-hydroxyindan-1-yl]-5-(5-methyl-4H-[1,2,4]triazol-3-yl)-pentanamide (25). Acetamidine hydrochloride (13.4 mg, 0.14 mmol) was dissolved in dry EtOH (0.5 mL), and sodium methoxide (7.6 mg, 0.14) was added. The mixture was stirred for 30 min, and the precipitated salt was filtered off. To the filtrate was added hydrazide **30** (56 mg, 0.094 mmol), and the resulting reaction mixture was stirred at reflux for 22 h. The reaction was monitored by TLC and analytical RP-LC-MS. The solvent was removed under reduced pressure, and subsequent purification by flash chromatography (0–5% MeOH in CHCl₃) gave **25** (19 mg, 33%) as a white solid: [α]_D¹⁹ +15.5° (*c* = 1.14, CHCl₃). Anal. (C₂₃H₂₈Br₂N₄O₆) C, H, N.

(2R,3R,4R,5R)-2,5-Bis[(2E)-3-(3,4-methylenedioxyphenyl)-2-propenyloxy]-3,4-dihydroxy-N1-[(1S,2R)-2-hydroxyindan-1-yl]-6-oxo-6-[N-(3-phenylpropionyl)hydrazino]-hexanamide (14). A mixture of diacyl hydrazine **9** (40 mg, 0.055 mmol), 3,4-methylenedioxyphenylboronic acid (55 mg, 0.33 mmol), Ba(OH)₂ × 8H₂O (60 mg, 0.19 mmol), Pd₂(dba)₃ (5.0 mg, 0.0055 mmol), [(*t*-Bu)₃PH]BF₄ (6.4 mg, 0.022 mmol), and DME/H₂O/EtOH, 12:4:3 (4 mL) was added to a heavy-walled Smith vial. The tube was capped and the mixture was stirred at 110 °C for 15 min in the microwave cavity. Consumption of starting material was checked by RP-LC-MS. The crude product was partitioned between CHCl₃ (50 mL) and 0.2 M HCl (aq) (30 mL). The organic layer was dried (Na₂SO₄) and concentrated. Purification by RP-LC-MS (30 min gradient of 30–77% CH₃CN in aqueous formic acid) gave **14** (10 mg, 23%) as a white solid: [α]_D²⁰ +34.7° (*c* = 0.39, MeOH). Anal. (C₄₄H₄₅N₃O₁₂) C, H, N.

(2R,3R,4R,5R)-2,5-Bis[(2E)-3-(4-acetylphenyl)-2-propenyloxy]-3,4-dihydroxy-N1-[(1S,2R)-2-hydroxyindan-1-yl]-

6-oxo-6-[N'-(3-phenylpropanoyl)hydrazino]-hexanamide (15). A mixture of diacyl hydrazine **9** (30 mg, 0.041 mmol), 4-acetylphenylboronic acid (41 mg, 0.25 mmol), Ba(OH)₂ × 8H₂O (46 mg, 0.14 mmol), Pd₂(dba)₃ (3.8 mg, 0.0041 mmol), [(*t*-Bu)₃PH]BF₄ (4.8 mg, 0.017 mmol), and DME/H₂O/EtOH, 12:4:3 (3 mL) was added to a heavy-walled Smith vial. The tube was capped, and the mixture was stirred at 110 °C for 40 min in the microwave cavity. Consumption of starting material was checked by RP-LC-MS. The crude product was partitioned between CHCl₃ (50 mL) and 0.2 M HCl (aq) (30 mL). The organic layer was dried (Na₂SO₄) and concentrated. Purification by RP-LC-MS (30 min gradient of 30–75% CH₃-CN in aqueous formic acid) gave **15** (7.4 mg, 22%) as a white solid: [α]_D²⁰ +28.7° (*c* = 0.66, MeOH). Anal. (C₄₆H₄₉N₃O₁₀) C, H, N.

Assays and K_i Determinations. Plm II was prepared according to Westling et al.,⁵⁸ and the expression and purification of Plm I will be published elsewhere (manuscript in preparation). The Plm IV assay was performed as described elsewhere.^{13,52} Human liver Cat D was purchased from Sigma-Aldrich, Sweden. The activities of Plm I, Plm II and Cat D were measured essentially as described earlier,²¹ using a total reaction volume of 100 μL. The concentration of pro-Plm II was 3 nM, the amount of Plm I was adjusted to give similar catalytic activity and 50 ng/mL pro-Cat D was used. The pro-sequence of Plm II was cleaved off by preincubation in assay reaction buffer (100 mM sodium acetate buffer (pH 4.5), 10% glycerol and 0.01% Tween 20) at room temperature for 40 min and Cat D was activated by incubation in the same reaction buffer at 37 °C for 20 min. The reaction was initiated by the addition of 3 μM substrate (DABCYL-Glu-Arg-Nle-Phe-Leu-Ser-Phe-Pro-EDANS, AnaSpec Inc, San Jose, CA), and hydrolysis was recorded as the increase in fluorescence intensity over a 10 min time period, during which the rate increased linearly with time. Stock solutions of inhibitors in DMSO were serially diluted in DMSO and added directly before addition of substrate, giving a final DMSO concentration of 1%. IC₅₀ values were obtained by assuming competitive inhibition and fitting Langmuir isotherm ($v_i/v_o = 1/(1 + [I]/IC_{50})$) to the dose response data (Grafite), where *v_i* and *v_o* are the initial velocities for the inhibited and uninhibited reaction respectively and [I] is the inhibitor concentration.⁵⁹ The K_i was subsequently calculated by using $K_i = IC_{50}/(1 + [S]/K_m)$ ⁶⁰ and a K_m value determined according to Michaelis–Menten.

The *P. falciparum*-infected erythrocyte assay was performed as described earlier.²⁶

MD Simulations and Free Energy Calculations. The linear interaction energy method (LIE)⁴⁵ is a useful tool for predicting absolute binding free energies of biomolecular complexes. According to this approach the free energy of binding can be estimated as:

$$\Delta G_{\text{bind}} = \alpha(\langle V_{1-s}^{\text{vdW}} \rangle_p - \langle V_{1-s}^{\text{vdW}} \rangle_w) + \beta(\langle V_{1-s}^{\text{el}} \rangle_p - \langle V_{1-s}^{\text{el}} \rangle_w) + \gamma(0.1)$$

where $\langle V_{1-s} \rangle$ is the thermodynamical average of the potential energy between the ligand and its surrounding environment. The subscripts p and w denote the calculated average of the ligand bound to the solvated receptor and free in solution, respectively, and the superscripts vdW and el denote the nonpolar (van der Waals) and polar (electrostatic) contributions to the potential energy average. The polar contribution is derived from the linear response approximation and depends on the chemical nature of the ligand. Here $\beta = 0.33$ was used as obtained in ref 61 for compounds with two or more hydroxyl groups. The nonpolar part of the potential energy is scaled by an empirically determined factor. As in ref 61 a value of 0.181 was used for α , and the constant γ was set to zero. Molecular dynamics (MD) trajectories were used to obtain the required averages, and the precision of these quantities was estimated by dividing the relevant trajectory in two halves and comparing their corresponding averages. The difference between them is the estimated error, which will be small for well equilibrated systems.

Reasonable starting structures for MD simulation are of importance for the convergence of binding free energy calculations. The ligand must thus initially be positioned relatively close to the native binding mode in order for the configurational sampling to converge around the true minimum within reasonable computing time. In earlier work we predicted the binding mode of compound **1** which has the same scaffold as the present ligands.²⁷ We were thus able to superimpose the compounds here onto the scaffold of **1** bound to Plm II from our earlier work and use that as a starting point for simulations. The Plm II X-ray structure in complex with pepstatin A was chosen as the starting protein model to take advantage of the fact that it is often easier to equilibrate a ligand–receptor complex by expanding a cavity rather than by collapsing it. Of the available Plm II X-ray models in complex with an inhibitor, the pepstatin A model was the most collapsed.

All MD calculations were done out with the Q package⁶² using the force field parameters of Gromos87.⁶³ Partial charges for the oxadiazole heterocyclic ring in ligand **23** and the vinyl bromide in **9** and **23** were calculated with the HF/6-31G* basis set after structure optimization with AM1 in Gaussian98.⁶⁴ All other atoms were assigned standard force field partial charges. Asp34 was protonated at the oxygen pointing toward Asp214. Asp214 was left unprotonated and was assigned a total charge of –1. The protonation and charge protocol was copied from earlier work.^{26,27}

The protein–ligand complexes were solvated in a 20 Å sphere of SPC water.⁶¹ The sphere was centered on the central carbon of the ligand closest to the P1' group. Water was added on a grid with a grid spacing of 3.1 Å and with a minimum distance of 2.4 Å to heavy atoms in the solute. Atoms outside the sphere were restrained to their initial positions with a harmonic potential with a force constant of 100 kcal/(mol Å²) and were only allowed to interact through bonded terms. All interactions involving ligand atoms were explicitly calculated within the sphere but for protein–protein, protein–water and water–water interactions a cutoff of 10 Å was applied. For long-range electrostatic interactions beyond this cutoff the local reaction field multipole expansion method⁶⁵ was used. Atoms in the outer shell of the simulation sphere, between 16 and 20 Å from the center, were weakly restrained with a force constant of 10 kcal/(mol Å²) to get a softer transition from restrained to unrestrained atoms across the sphere boundary.

The systems were equilibrated by slowly raising the temperature from 1 to 300 K in five steps. Loose restraints were used to keep the four hydrogen bonds involved in the extended β conformation between the ligands and the protein intact. The two central hydroxyls of the ligands interacting with the catalytic dyad, Asp34 and Asp214, were also kept in place with restraints during the equilibration. The restrained equilibration was performed for 100 ps with gradually decreasing restraints, increasing time step and increasing temperature. A time step of 0.2 fs was used in the initial equilibration and was increased to a final value of 1.0 fs. The systems were finally subjected to unrestrained equilibration of at least 500 ps before data collection. During data collection energies were recorded every 25 fs and energy averaging was done on more than 1 ns of MD.

The simulations of the ligands in the unbound state were performed in a similar manner. The ligands were solvated in a 20 Å radius and were equilibrated for 50 ps at 300 K. The geometrical centers of the ligands were restrained to the center of the sphere by a harmonic potential of 50 kcal/(mol Å²) to keep the ligands from drifting out toward the boundary of the sphere. Radial and polarization restraints⁶⁶ were applied to the water in all simulations to mimic bulk water at the sphere boundary. Time averaging was done on trajectories of more than 1 ns.

Rigid receptor docking was carried out with Autodock3.⁴⁶ The dockings were made with ligand **16** using 10 million energy calculations per run and a population of 150 individuals. Being the smallest ligand in the computational evaluated set it is more likely than the other to fit into a rigid binding

site. The 1SME, 1LF2 and 1LF3 X-ray structures were used as models of Plm II and were initially processed with the standard Autodock procedure. In a final step the hydrogen used in our simulations on Asp214 was added manually and the partial charges of Asp214 were modified to the protonated Asp residue in the AMBER95 force field.⁶⁷ The ligand was assigned Gasteiger charges as implemented in Autodock. The rigid root was picked automatically and all amide bonds were kept rigid through the conformational search. One hundred fifty separate runs were made in each protein model, and the results were clustered with an RMSD of 2.5 Å.

Additional dockings were made where the C ϵ of Met75 in 1SME and 1LF3 moved by a 180° rotation around the C β –C γ –S δ –C ϵ torsion, thereby enlarging the S2' pocket. In the 1LF2 model of PlmII the S2' is already in the open conformation, and hence no rotation was made there.

Acknowledgment. We thank the Swedish Foundation for Strategic Research (SSF) and the Swedish Research Council (VR) for financial support. We also thank Biotage for providing a Smith Synthesizer.

Supporting Information Available: ¹H and ¹³C NMR spectra of the compounds 3–25 and 28–30. This information is available free of charge via the Internet at <http://pubs.acs.org>.

References

- Breman, J. The Ears of the Hippopotamus: Manifestations, Determinants, and Estimates of the Malaria Burden. *Am. J. Trop. Med. Hyg.* **2001**, *64* (1, 2/S), 1–11.
- Wongsrichanalai, C.; Pickard, A. L.; Wernsdorfer, W. H.; Meshnick, S. R. Epidemiology of Drug-Resistant Malaria. *Lancet Infect. Dis.* **2002**, *2*, 209–218.
- Gardner, M. J.; Hall, N.; Fung, E.; White, O.; Berriman, M.; Hyman, R. W.; Carlton, J. M.; Pain, A.; Nelson, K. E.; Bowman, S.; Paulsen, I. T.; James, K.; Eisen, J. A.; Rutherford, K.; Salzberg, S. L.; Craig, A.; Kyes, S.; Chan, M.-S.; Nene, V.; Shallom, S. J.; Suh, B.; Peterson, J.; Angiuoli, S.; Perete, M.; Allen, J.; Selengut, J.; Haft, D.; Mather, M. W.; Vaidya, A. B.; Martin, D. M. A.; Fairlamb, A. H.; Fraunholz, M. J.; Roos, D. S.; Ralph, S. A.; McFadden, G. I.; Cummings, L. M.; Subramanian, G. M.; Mungall, C.; Venter, J. C.; Carucci, D. J.; Hoffman, S. L.; Newbold, C.; Davis, R. W.; Fraser, C. M.; Barrell, B. Genome Sequence of the Human Malaria Parasite *Plasmodium falciparum*. *Nature (London)* **2002**, *419*, 498–511.
- Banerjee, R.; Liu, J.; Beatty, W.; Pelosof, L.; Klemba, M.; Goldberg, D. E. Four Plasmepepsins are Active in the *Plasmodium falciparum* Food Vacuole, Including a Protease with an Active-Site Histidine. *Proc. Natl. Acad. Sci. U.S.A.* **2002**, *99*, 990–995.
- Rosenthal, P. J. *Plasmodium falciparum*: Effects of Proteinase Inhibitors on Globin Hydrolysis by Cultured Malaria Parasites. *Exp. Parasitol.* **1995**, *80*, 272–281.
- Olson, J. E.; Lee, G. K.; Semenov, A.; Rosenthal, P. J. Antimalarial Effects in Mice of Orally Administered Peptidyl Cysteine Protease Inhibitors. *Bioorg. Med. Chem. Lett.* **1999**, *7*, 633–638.
- Boss, C.; Richard-Bildstein, S.; Weller, T.; Fischli, W.; Meyer, S.; Binkert, C. Inhibitors of the *Plasmodium falciparum* Parasite Aspartic Protease Plasmepepsin II as Potential Antimalarial Agents. *Curr. Med. Chem.* **2003**, *10*, 883–907.
- Salas, F.; Fichmann, J.; Lee, G. K.; Scott, M. D.; Rosenthal, P. J. Functional Expression of Falcipain, a *Plasmodium falciparum* Cysteine Proteinase, Supports its Role as a Malarial Hemoglobinase. *Infect. Immun.* **1995**, *63*, 2120–2125.
- Shenai, B. R.; Sijwali, P. S.; Singh, A.; Rosenthal, P. J. Characterization of Native and Recombinant Falcipain-2, a Principal Trophozoite Cysteine Protease and Essential Hemoglobinase of *Plasmodium falciparum*. *J. Biol. Chem.* **2000**, *275*, 29000–29010.
- Sijwali, P. S.; Shenai, B. R.; Gut, J.; Singh, A.; Rosenthal, P. J. Expression and characterization of the *Plasmodium falciparum* hemoglobinase falcipain-3. *Biochem. J.* **2001**, *360*, 481–489.
- Eggleston, K. K.; Duffin, K. L.; Goldberg, D. E. Identification and Characterization of Falcilysin, a Metalloproteinase Involved in Hemoglobin Catabolism within the Malaria Parasite *Plasmodium falciparum*. *J. Biol. Chem.* **1999**, *274*, 32411–32417.
- Nezami, A.; Kimura, T.; Hidaka, K.; Kiso, A.; Liu, J.; Kiso, Y.; Goldberg, D. E.; Freire, E. High-Affinity Inhibition of a Family of *Plasmodium falciparum* Proteases by a Designed Adaptive Inhibitor. *Biochemistry* **2003**, *42*, 8459–8464.
- Dame, J. B.; Yowell, C. A.; Omara-Opyene, L.; Carlton, J. M.; Cooper, R. A.; Li, T. Plasmepepsin 4, the Food Vacuole Aspartic Proteinase Found in all *Plasmodium* Spp. Infecting Man. *Mol. Biochem. Parasitol.* **2003**, *130*, 1–12.
- Wyatt David, M.; Berry, C. Activity and inhibition of plasmepepsin IV, a new aspartic proteinase from the malaria parasite, *Plasmodium falciparum*. *FEBS Lett.* **2002**, *513*, 159–162.
- Bjelic, S.; Aqvist, J. Computational Prediction of Structure, Substrate Binding Mode, Mechanism, and Rate for a Malaria Protease with a Novel Type of Active Site. *Biochemistry* **2004**, *43*, 14521–14528.
- Nezami, A.; Freire, E. The Integration of Genomic and Structural Information in the Development of High Affinity Plasmepepsin Inhibitors. *Int. J. Parasitol.* **2002**, *32*, 1669–1676.
- Goldberg, D. E.; Slater, A. F. G.; Beavis, R.; Chait, B.; Cerami, A.; Henderson, G. B. Hemoglobin Degradation in the Human Malaria Pathogen *Plasmodium falciparum*: A Catabolic Pathway Initiated by a Specific Aspartic Protease. *J. Exp. Med.* **1991**, *173*, 961–969.
- Gluzman, I. Y.; Francis, S. E.; Oksman, A.; Smith, C. E.; Duffin, K. L.; Goldberg, D. E. Order and Specificity of the *Plasmodium falciparum* Hemoglobin Degradation Pathway. *J. Clin. Invest.* **1994**, *93*, 1602–1608.
- Silva, A. M.; Lee, A. Y.; Gulnik, S. V.; Majer, P.; Collins, J.; Bhat, T. N.; Collins, P. J.; Cachau, R. E.; Luker, K. E.; Gluzman, I. Y.; Francis, S. E.; Oksman, A.; Goldberg, D. E.; Erickson, J. W. Structure and Inhibition of Plasmepepsin II, a Hemoglobin-Degrading Enzyme from *Plasmodium falciparum*. *Proc. Natl. Acad. Sci. U.S.A.* **1996**, *93*, 10034–10039.
- Moon, R. P.; Tyas, L.; Certa, U.; Rupp, K.; Bur, D.; Jacquet, C.; Matile, H.; Loetscher, H.; Grueninger-Leitch, F.; Kay, J.; Dunn, B. M.; Berry, C.; Ridley, R. G. Expression and Characterization of Plasmepepsin I from *Plasmodium falciparum*. *Eur. J. Biochem.* **1997**, *244*, 552–560.
- Haque, T. S.; Skillman, A. G.; Lee, C. E.; Habashita, H.; Gluzman, I. Y.; Ewing, T. J. A.; Goldberg, D. E.; Kuntz, I. D.; Ellman, J. A. Potent, Low-Molecular-Weight Non-Peptide Inhibitors of Malarial Aspartyl Protease Plasmepepsin II. *J. Med. Chem.* **1999**, *42*, 1428–1440.
- Nöteberg, D.; Hamelink, E.; Hultén, J.; Wahlgren, M.; Vrang, L.; Samuelsson, B.; Hallberg, A. Design and Synthesis of Plasmepepsin I and Plasmepepsin II Inhibitors with Activity in *Plasmodium falciparum*-Infected Cultured Human Erythrocytes. *J. Med. Chem.* **2003**, *46*, 734–746.
- Dahlgren, A.; Kvarnstrom, I.; Vrang, L.; Hamelink, E.; Hallberg, A.; Rosenquist, A.; Samuelsson, B. New Inhibitors of the Malaria Aspartyl Proteases Plasmepepsin I and II. *Bioorg. Med. Chem.* **2003**, *11*, 3423–3437.
- Oscarsson, K.; Oscarson, S.; Vrang, L.; Hamelink, E.; Hallberg, A.; Samuelsson, B. New Potent C₂-Symmetric Malaria Plasmepepsin I and II Inhibitors. *Bioorg. Med. Chem.* **2003**, *11*, 1235–1246.
- Nöteberg, D.; Schaal, W.; Hamelink, E.; Vrang, L.; Larhed, M. High-speed Optimization of Inhibitors of the Malarial Proteases Plasmepepsin I and II. *J. Comb. Chem.* **2003**, *5*, 456–464.
- Ersmark, K.; Feierberg, I.; Bjelic, S.; Hamelink, E.; Hackett, F.; Blackman, M. J.; Hultén, J.; Samuelsson, B.; Aqvist, J.; Hallberg, A. Potent Inhibitors of the *Plasmodium falciparum* Enzymes Plasmepepsin I and II Devoid of Cathepsin D Inhibitory Activity. *J. Med. Chem.* **2004**, *47*, 110–122.
- Ersmark, K.; Feierberg, I.; Bjelic, S.; Hultén, J.; Samuelsson, B.; Aqvist, J.; Hallberg, A. C₂-Symmetric Inhibitors of *Plasmodium falciparum* Plasmepepsin II: Synthesis and Theoretical Predictions. *Bioorg. Med. Chem.* **2003**, *11*, 3723–3733.
- Carroll, C. D.; Patel, H.; Johnson, T. O.; Guo, T.; Orłowski, M.; He, Z.-M.; Cavallaro, C. L.; Guo, J.; Oksman, A.; Gluzman, I. Y.; Connelly, J.; Chelsky, D.; Goldberg, D. E.; Dolle, R. E. Identification of Potent Inhibitors of *Plasmodium falciparum* Plasmepepsin II from an Encoded Statine Combinatorial Library. *Bioorg. Med. Chem. Lett.* **1998**, *8*, 2315–2320.
- Carroll, C. D.; Johnson, T. O.; Tao, S.; Lauri, G.; Orłowski, M.; Gluzman, I. Y.; Goldberg, D. E.; Dolle, R. E. Evaluation of a Structure-Based Statine Cyclic Diamino Amide Encoded Combinatorial Library Against Plasmepepsin II and Cathepsin D. *Bioorg. Med. Chem. Lett.* **1998**, *8*, 3203–3206.
- Dolle, R. E.; Guo, J.; O'Brien, L.; Jin, Y.; Piznik, M.; Bowman, K. J.; Li, W.; Egan, W. J.; Cavallaro, C. L.; Roughton, A. L.; Zhao, W.; Reader, J. C.; Orłowski, M.; Jacob-Samuel, B.; DiIanni Carroll, C. A Statistical-Based Approach to Assessing the Fidelity of Combinatorial Libraries Encoded with Electrophoric Molecular Tags. Development and Application of Tag Decode-Assisted Single Bead LC/MS Analysis. *J. Comb. Chem.* **2000**, *2*, 716–731.
- Jiang, S.; Prigge, S. T.; Wei, L.; Gao, Y.-E.; Hudson, T. H.; Gerena, L.; Dame, J. B.; Kyle, D. E. New Class of Small Nonpeptidyl Compounds Blocks *Plasmodium falciparum* Development In Vitro by Inhibiting Plasmepepsins. *Antimicrob. Agents Chemother.* **2001**, *45*, 2577–2584.
- Nezami, A.; Luque, I.; Kimura, T.; Kiso, Y.; Freire, E. Identification and Characterization of Allophenylnorstatine-Based Inhibitors of Plasmepepsin II, an Antimalarial Target. *Biochemistry* **2002**, *41*, 2273–2280.

- (33) Asojo, O. A.; Afonina, E.; Gulnik, S. V.; Yu, B.; Erickson, J. W.; Randad, R.; Medjahed, D.; Silva, A. M. Structures of Ser205 Mutant Plasmepepsin II from *Plasmodium falciparum* at 1.8 Å in Complex with the Inhibitors rs367 and rs370. *Acta Crystallogr. D* **2002**, *D58*, 2001–2008.
- (34) Johansson, P.-O.; Chen, Y.; Belfrage, A. K.; Blackman, M. J.; Kvarnstrom, I.; Jansson, K.; Vrang, L.; Hamelink, E.; Hallberg, A.; Rosenquist, A.; Samuelsson, B. Design and Synthesis of Potent Inhibitors of the Malaria Aspartyl Proteases Plasmepepsin I and II. Use of Solid-Phase Synthesis to Explore Novel Statine Motifs. *J. Med. Chem.* **2004**, *47*, 3353–3366.
- (35) Berry, C. Plasmepepsins as Antimalarial Targets. *Curr. Opin. Drug Discovery Des.* **2000**, *3*, 624–629.
- (36) Patani, G. A.; LaVoie, E. J. Bioisosterism: A Rational Approach in Drug Design. *Chem. Rev.* **1996**, *96*, 3147–3176.
- (37) Chen, X.; Wang, W. The Use of Bioisosteric Groups in Lead Optimization. *Annu. Rep. Med. Chem.* **2003**, *38*, 333–346.
- (38) Giannis, A.; Kolter, T. Peptide Mimetics for Receptor Ligands: Discovery, Development, and Medicinal Perspectives. *Angew. Chem.* **1993**, *105*, 1303–1326.
- (39) Asojo, O. A.; Gulnik, S. V.; Afonina, E.; Yu, B.; Ellman, J. A.; Haque, T. S.; Silva, A. M. Novel Uncomplexed and Complexed Structures of Plasmepepsin II, an Aspartic Protease from *Plasmodium falciparum*. *J. Mol. Biol.* **2003**, *327*, 173–181.
- (40) Brain, C. T.; Paul, J. M.; Loong, Y.; Oakley, P. J. Novel Procedure for the Synthesis of 1,3,4-Oxadiazoles from 1,2-Diacylhydrazines Using Polymer-Supported Burgess Reagent under Microwave Conditions. *Tetrahedron Lett.* **1999**, *40*, 3275–3278.
- (41) Oscarsson, K.; Lahmann, M.; Lindberg, J.; Kangasmetza, J.; Unge, T.; Oscarson, S.; Hallberg, A.; Samuelsson, B. Design and Synthesis of HIV-1 Protease Inhibitors. Novel Tetrahydrofuran P2/P2'-Groups Interacting with Asp29/30 of the HIV-1 Protease. Determination of Binding from X-ray Crystal Structure of Inhibitor Protease Complex. *Bioorg. Med. Chem.* **2003**, *11*, 1107–1115.
- (42) Larhed, M.; Moberg, C.; Hallberg, A. Microwave-Accelerated Homogeneous Catalysis in Organic Chemistry. *Acc. Chem. Res.* **2002**, *35*, 717–727.
- (43) Larhed, M.; Lindeberg, G.; Hallberg, A. Rapid Microwave-Assisted Suzuki Coupling on Solid-Phase. *Tetrahedron Lett.* **1996**, *37*, 8219–8222.
- (44) Netherton, M. R.; Fu, G. C. Air-Stable Trialkylphosphonium Salts: Simple, Practical, and Versatile Replacements for Air-Sensitive Trialkylphosphines. Applications in Stoichiometric and Catalytic Processes. *Org. Lett.* **2001**, *3*, 4295–4298.
- (45) Aqvist, J.; Medina, C.; Samuelsson, J. E. A New Method for Predicting Binding Affinity in Computer-Aided Drug Design. *Protein Eng.* **1994**, *7*, 385–391.
- (46) Morris, G. M.; Goodsell, D. S.; Halliday, R. S.; Huey, R.; Hart, W. E.; Belew, R. K. and Olson, A. J. Automated Docking Using a Lamarckian Genetic Algorithm and Empirical Binding Free Energy Function. *J. Comput. Chem.* **1998**, *19*, 1639–1662.
- (47) Hulten, J.; Bonham, N. M.; Nillroth, U.; Hansson, T.; Zuccarello, G.; Bouzide, A.; Aqvist, J.; Classon, B.; Danielson, U. H.; Karlen, A.; Kvarnstrom, I.; Samuelsson, B.; Hallberg, A. Cyclic HIV-1 Protease Inhibitors Derived from Mannitol: Synthesis, Inhibitory Potencies, and Computational Predictions of Binding Affinities. *J. Med. Chem.* **1997**, *40*, 885–897.
- (48) Kuntz, I. D.; Chen, K.; Sharp, K. A.; Kollman, P. A. The Maximal Affinity of Ligands. *Proc. Natl. Acad. Sci. U.S.A.* **1999**, *96*, 9997–10002.
- (49) Shirts, M. R.; Pitner, J. W.; Swope, W. C.; Pande, V. S. Extremely Precise Free Energy Calculations of Amino Acid Side Chain Analogues: Comparison of Common Molecular Mechanics Force Fields for Proteins. *J. Chem. Phys.* **2003**, *119*, 5740–5761.
- (50) Oostenbrink, C.; Villa, A.; Mark, A. E.; van Gunsteren, W. F. A Biomolecular Force Field Based on the Free Enthalpy of Hydration and Solvation: The GROMOS Force-Field Parameter Sets 53A5 and 53A6. *J. Comput. Chem.* **2004**, *25*, 1656–1676.
- (51) Coombs, G. H.; Goldberg, D. E.; Klemba, M.; Berry, C.; Kay, J.; Motttram, J. C. Aspartic Proteases of *Plasmodium falciparum* and other Parasitic Protozoa as Drug Targets. *Trends Parasitol.* **2001**, *17*, 532–537.
- (52) Li, T. Y.; C. A.; Beyer, B. B.; Hung, S.-H.; Westling, J.; Lam, M. T.; Dunn, B. M.; Dame, J. B. Recombinant Expression and Enzymatic Subsite Characterization of Plasmepepsin 4 from the Four *Plasmodium* Species Infecting Man. *Mol. Biochem. Parasitol.* **2004**, *135*, 101–109.
- (53) Omara-Opyene, A. L.; Moura, P. A.; Sulsona, C. R.; Bonilla, J. A.; Yowell, C. A.; Fujioka, H.; Fidock, D. A.; Dame, J. B. Genetic Disruption of the *Plasmodium falciparum* Digestive Vacuole Plasmepepsins Demonstrates Their Functional Redundancy. *J. Biol. Chem.* **2004**, *279*, 54088–54096.
- (54) Liu, J.; Gluzman, I. Y.; Drew, M. E.; Goldberg, D. E. The Role of *Plasmodium falciparum* Food Vacuole Plasmepepsins. *J. Biol. Chem.* **2005**, *280*, 1432–1437.
- (55) Prata, J. V.; Clemente, D.-T. S.; Prabhakar, S.; Lobo, A. M.; Mourato, I.; Branco, P. S. Intramolecular Addition of Acyldiaz-enecarboxylates Onto Double Bonds in the Synthesis of Heterocycles. *J. Chem. Soc., Perkin Trans. 1* **2002**, 513–528.
- (56) Henichart, J. P.; Houssin, R.; Lablanche, B. Synthesis and Structure of 1,2,4-Triazolone-5-thiones Having a Dialkylamino-ethyl Substituent at the 3 or 4 Position. *J. Heterocycl. Chem.* **1977**, *14*, 615–619.
- (57) Massarani, E.; Nardi, D.; Rossi, S.; Tajana, A.; Degen, L. Antibacterial Nitrofurans Derivatives. 3. 5-Nitro-2-furaldehyde Piperazinoacylhydrazones. *J. Med. Chem.* **1971**, *14*, 635–638.
- (58) Westling, J.; Cipullo, P.; Hung, S. H.; Saft, H.; Dame, J. B.; Dunn, B. M. Active Site Specificity of Plasmepepsin II. *Protein Sci.* **1999**, *8*, 2001–2009.
- (59) Copeland, R. A.; Ed. *Enzymes: A Practical Introduction to Structure, Mechanism, and Data Analysis*; VCH: New York, 1996; 300 pp.
- (60) Cheng, Y.; Prusoff, W. H. Relationship Between the Inhibition Constant (K_I) and the Concentration of Inhibitor which Causes 50 Per Cent Inhibition (I₅₀) of an Enzymatic Reaction. *Biochem. Pharmacol.* **1973**, *22*, 3099–3108.
- (61) Marelus, J.; Hansson, T.; Aqvist, J. Calculation of Ligand Binding Free Energies from Molecular Dynamics Simulations. *Int. J. Quantum Chem.* **1998**, *69*, 77–88.
- (62) Marelus, J.; Kolmodin, K.; Feierberg, I.; Aqvist, J. Q: A Molecular Dynamics Program for Free Energy Calculations and Empirical Valence Bond Simulations in Biomolecular Systems. *J. Mol. Graph. Model.* **1998**, *16*, 213–225, 261.
- (63) van Gunsteren, W. F. B.; H. J. C. *Groningen Molecular Simulation (GROMOS) Library Manual*; Nijenborgh: Groningen, The Netherlands, 1997.
- (64) Frisch, M. J.; Trucks, G. W.; Schlegel, H. B.; Scuseria, G. E.; Robb, M. A.; Cheeseman, J. R.; Zakrzewski, V. G.; Montgomery, J. A., Jr.; Stratmann, R. E.; Burant, J. C.; Dapprich, S.; Millam, J. M.; Daniels, A. D.; Kudin, K. N.; Strain, M. C.; Farkas, O.; Tomasi, J.; Barone, V.; Cossi, M.; Cammi, R.; Mennucci, B.; Pomelli, C.; Adamo, C.; Clifford, S.; Ochterski, J.; Petersson, G. A.; Ayala, P. Y.; Cui, Q.; Morokuma, K.; Malick, D. K.; Rabuck, A. D.; Raghavachari, K.; Foresman, J. B.; Cioslowski, J.; Ortiz, J. V.; Stefanov, B. B.; Liu, G.; Liashenko, A.; Piskorz, P.; Komaromi, I.; Gomperts, R.; Martin, R. L.; Fox, D. J.; Keith, T.; Al-Laham, M. A.; Peng, C. Y.; Nanayakkara, A.; Gonzalez, C.; Challacombe, M.; Gill, P. M. W.; Johnson, B. G.; Chen, W.; Wong, M. W.; Andres, J. L.; Head-Gordon, M.; Replogle, E. S.; Pople, J. A. *Gaussian 98*, revision x.x; Gaussian, Inc.: Pittsburgh, PA, 1998.
- (65) Lee, F. S.; Warshel, A. A Local Reaction Field Method for Fast Evaluation of Long-Range Electrostatic Interactions in Molecular Simulations. *J. Chem. Phys.* **1992**, *97*, 3100–3107.
- (66) King, G.; Warshel, A. A Surface-Contained All-Atom Solvent Model for Effective Simulations of Polar Solutions. *J. Chem. Phys.* **1989**, *91*, 3647–3661.
- (67) Cornell, W. D.; Cieplak, P.; Bayly, C. I.; Gould, I. R.; Merz, K. M., Jr.; Ferguson, D. M.; Spellmeyer, D. C.; Fox, T.; Caldwell, J. W.; Kollman, P. A. A Second Generation Force Field for the Simulation of Proteins, Nucleic Acids, and Organic Molecules. *J. Am. Chem. Soc.* **1996**, *118*, 2309.

JM050463L